Title
Optimized Mixing in Microchannels with Integrated Microactuators

Author
Folk, Christopher

Publication Date
2014

Peer reviewed|Thesis/dissertation

UNIVERSITY OF CALIFORNIA

Los Angeles

Optimized Mixing in Microchannels with Integrated Microactuators

A dissertation submitted in partial satisfaction of the

requirements for the degree Doctor of Philosophy

in Aerospace Engineering

by

Christopher Richard Folk

2014

ABSTRACT OF THE DISSERTATION

Optimized Mixing in Microchannels with Integrated Microactuators

by

Christopher Richard Folk

Doctor of Philosophy in Aerospace Engineering

University of California, Los Angeles, 2014

Professor Chih-Ming Ho, Chair

Microscale valves and pumps have been designed and fabricated for integration into a microfluidic circuit. Furthermore, a micromixer for this circuit has been designed and optimized. N-isopropylacrylamide (NIPA) gels have been fabricated and actuated directly with heat and indirectly by laser. A new method for photopatterning these gels based on photoinitiation has been used to fabricate hydrogel valves down to 50 μm in diameter. Hydrogel valves have been fabricated in situ in a microfluidic network. The valves open in 27 seconds and close via diffusion of water into the gel in 128 seconds, which is faster than other optically-driven polymers used for large displacements.

In this research, azobis-isobutyronitrile (AIBN) is incorporated into a variety of polydimethylsiloxane (PDMS) pump chambers. The AIBN is heated via integrated resistive

heaters and decomposes to release nitrogen gas. The nitrogen gas provides impulse power to a PDMS diaphragm to displace the fluid. The pump devices have been built and characterized. Lastly, in this work, we describe the use of combined fluid dynamic and diffusion modeling to simulate a micromixer based on the elements above. The micromixer is optimized via Design of Experiments to produce an optimized geometry for mixing. The optimization is validated via comparison to previous work through the Strouhal number.

The dissertation of Christopher Richard Folk is approved.

Yong Chen

Chang-Jin Kim

Dean Ho

Chih-Ming Ho, Committee Chair

University of California, Los Angeles

2014

Table of Contents

ACKNOWLEDGEMENTS

First and foremost, I would like to express my gratitude to advisor and committee chairman, Professor Chih-Ming Ho for his instruction and support at UCLA. In addition to the direct financial support and mentorship over the years, Dr. Ho has done me a far greater service by serving as true role model of character and intellectual courage. He sets a high bar. I would like to thank both current and former members of the lab members affectionately referred to as "Team Ho". In addition to professional peers, multiple lifelong friendships were based on our work together. Joann Deval, Steven Ho, Hiroaki Suzuki, and Jeff Tza-Huei Wang were great partners during the preliminary exam period. Adam Huang was a tremendous researcher in our early Aero-MEMS work. Yifhar Chen and Joon Mo Ma provided key early guidance. More recently, Yi-Kuen Lee lent key insight to the work throughout this thesis, and his work is used to validate many of the elements hereafter. A special thanks is due to Yanbao Ma, who developed early computational fluid dynamic models of micromixers based on the pump design, and had the insight to realize the numerical challenges of matching time and space discretization when solving both Navier-Stokes and the convective-diffusion equation. Pak Kin Wong has been a key collaborator from this work's inception to the current period. In the current period, Hann Wang offered timely insight to optimization routines.

Outside of our immediate lab, Xiangxu Chen and Fred Wudl were key partners in the development of hydrogel actuators. Xiangxu in particular demonstrated exemplary patience and continues to be a great colleague.

I'm honored to have Professors CJ Kim, Dean Ho, and Yong Chen on my committee. All are

exemplary scientists and engineers, and Prof. Yong Chen has been a singular example of courage on behalf of the people of China. I'm also grateful to Steve Franz and the staff of the UCLA Nanofabrication facility.

Lastly, I would like to thank my family, my wonderful wife Jody, and the extraordinary friends who have supported us over the years. I moved to Los Angeles to receive an education, and in the process, Jody and I found one another and created a home.

VITA

1995	Bachelor of Science, Department of Aerospace Engineering
	University of Notre Dame
1995-1998	General Electric, Aircraft Engines
	Technical Leadership Program
1996-1998	Master of Science, Engineering Mechanics
	University of Cincinnati
1998-2005	University of California, Los Angeles
	Research Assistant
2000-2010	Microfabrica
	Senior MEMS Design Engineer
2010-2013	ev3 / Covidien
	R&D Manager, Neurovascular Access
2013-present	Amgen
	Principal Engineer, Device Strategy

JOURNAL PUBLICATIONS AND PATENTS

1. Vasilyev NV, Gosline A, Butler E, Lang N, Codd P, Yamauchi H, Feins E, Folk C, Cohen A, Chen R, del Nido PJ, Dupont PE, "Percutaneous Steerable Robotic Tool Delivery Platform and Metal MEMS Device for Tissue Manipulation and Approximation: Initial Experience with Closure of Patent Foramen Ovale", *Circulation: Cardiovascular Interventions*, 2013.
2. Gosline AH, Vasilyev NV, Butler EJ, Folk C, Cohen A, Chen R, Lang N, Del Nido PJ, Dupont PE, "Percutaneous intracardiac beating-heart surgery using metal MEMS tissue approximation tools", *International Journal of Robotics Research*, 31(9) 1081-1093, August 2012.
3. Vasilyev NV, Lang N, Yamauchi H, Folk CR, Cohen AL, Chen R, del Nido PJ, Dupont PE. "Image- Guided Beating-Heart Closure of Patent Foramen Ovale Using Novel MEMS Closure Device". Transcatheter Therapeutics (TCT) 2010, September 21-25, Washington, DC. *J. Am. Coll. Cardiol.* 2010;56;B30.
4. Cohen A, Chen R, Frodis U, Wu M, Folk C. "Microscale metal additive manufacturing of multi- component medical devices" *Rapid Prototyping Journal*, Vol 16, No3, 2010. pp 209-215.

1. US Patent #8511960 Microscale and millimeter scale devices including threaded elements, methods for designing, and methods for making
2. US Patent #8454652 Releasable Tissue Anchoring Device, Methods for Using, and Methods for Making
3. US Patent #8241228 Micro-scale and meso-scale hydraulic and pneumatic tools, methods for using, and methods for making
4. US Patent #7567089 Two-part microprobes for contacting electronic components and methods for making such probes

Chapter 1

INTRODUCTION

1.1 Objective

Current micromachined pumps and valves are not particularly robust and are difficult to integrate with an optical sensor. A simple microfluidic network regulated by hydrogel valves and gas-emitting pumps is conceived as a simple alternative to complicated mechanical valves. Light and heat are commonly used in lab-on-a-chip systems. The valves and pumps in this system must be driven optically or thermally to allow for reconfigurability and addressability. The motivation of the research in optically and thermally driven fluidics is to create a totally integrated system that may use the same power source as the detection subsystem. Three fluidic elements must be created for a complete lab-on-a-chip system: valves, pumps, and a mixer.

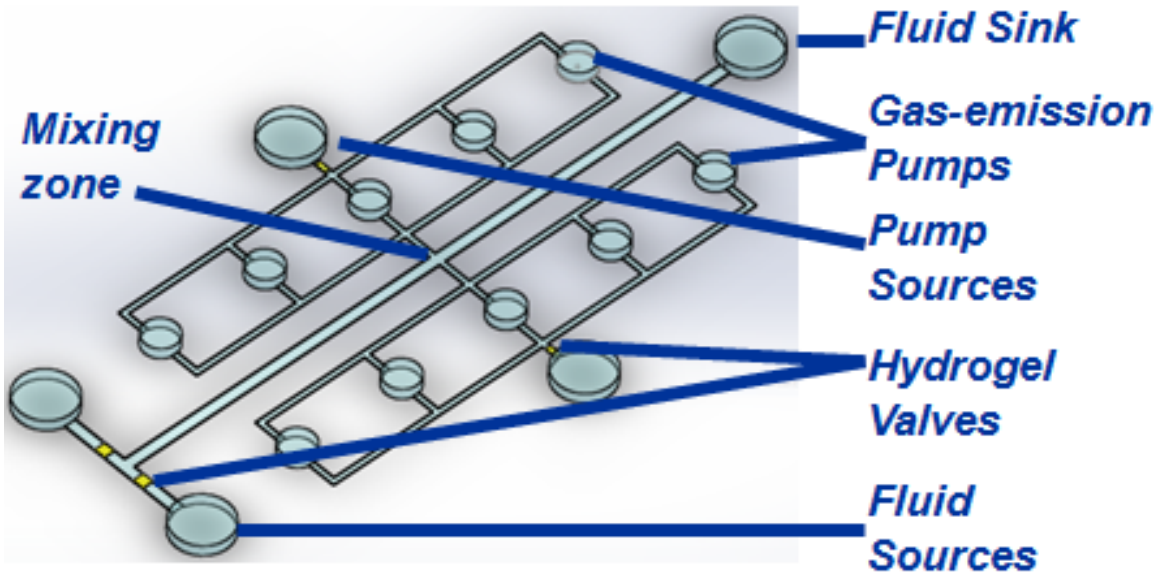

Figure 1: Goal of integrated micropumps, valves, and micromixer for Lab-on-a-Chip

1.2 Thesis Overview

The goal of this research is to develop polymeric actuators valuable for pumps, valves, and mixers in a disposable microfluidic platform for point-of-care diagnostics. The heterogeneous nature of biological samples renders commonly used transport mechanisms, such as capillary electrophoresis or electrowetting, subject to fouling in microchannels. Thus, mechanical forces generated by thermal or optical polymer actuators are chosen to drive the fluid and enable mixing.

Hydrogels based on N-isopropylacrylamide (NIPA) undergo a phase transition at 34^0C from a hydrophilic state to a hydrophobic state and lose 53% or more of their volume while releasing water. This mechanism simply requires heat and is particularly useful for actuation in the microscale because the time constant scales to the linear dimension of the gel. Differential scanning calorimetry tests indicate a wide variety of dyes may be incorporated into these hydrogels. These dyes transduce laser energy to heat and actuate the hydrogel. Thus, fluidic actuation may be driven by different wavelengths of light. Microscale NIPA gels have been fabricated and actuated directly with heat and indirectly by laser. A new method for photopatterning these gels based on photoinitiation has been used to fabricate hydrogel valves down to 50 um in diameter. Hydrogel valves have been fabricated in situ in a microfluidic network. The valves open in 27 seconds and close via diffusion of water into the gel in 128 seconds, which is faster than other optically-driven polymers used for large displacements.

Powerful pumps are key elements of an effective microfluidic network. Numerous micromachined pump elements have been demonstrated to date. To advance the field, low cost, easily fabricated pumps are required to generate high pressure quickly. Solid propellants offer one solution. In this research, azobis-isobutyronitrile (AIBN) is incorporated into a variety of polydimethylsiloxane (PDMS) pump chambers. The AIBN is heated via integrated resistive heaters. Once the AIBN reaches a range of 65-95^{0}C, the AIBN rapidly decomposes to release nitrogen gas. The nitrogen gas provides impulse power to a PDMS diaphragm to displace the fluid. These pump devices have been built and characterized.

Lastly, low-cost, efficient mixing at the microscale remains a challenge, although a wide variety of micromixers have been designed and fabricated. In this work, we describe the use of combined fluid dynamic and diffusion modeling to simulate a micromixer based on the elements above. Furthermore, the micromixer is optimized via Design of Experiments to produce an optimized geometry for mixing.

Chapter 2

HYDROGEL ACTUATORS

2.1 Lab-on-a-Chip Context

Two goals of microfluidic and nanofluidic research are to more completely understand the science of fluids on small length scales and to enable lab-on-a-chip systems. Lab-on-a-chip technology may be applied for such beneficial purposes as biowarfare detection, environmental monitoring, drug discovery, and point-of-care diagnostics. The success of lab-on-chip systems will depend on the versatility, accuracy, and cost effectiveness of the underpinning flow control technologies. The appeal of this technology is for sensitive, specific and rapid detection.

For many point-of-care diagnostics, the goal is to quantify, identify, or extract information from cells. Typical cells of interest such as bacteria may be in liquid media or airborne. If the cells are airborne, an effective means must be used to introduce the cells to the fluidic circuit. Typical raw samples from the environment require several fluidic processes to yield the information rich biomolecules needed for identification of bacteria. Fluidic processes used in lab-on-a-chip systems include filtration, pumping, valving, mixing, and concentration. These processes may be repeated several times in the sample-to-solution protocol. For example, in a bench top minisystem[1] used to identify and quantify E. coli bacteria, three peristaltic pumps and five valves were required to release and identify target DNA molecules from an intact bacterium as shown in Figure 2.

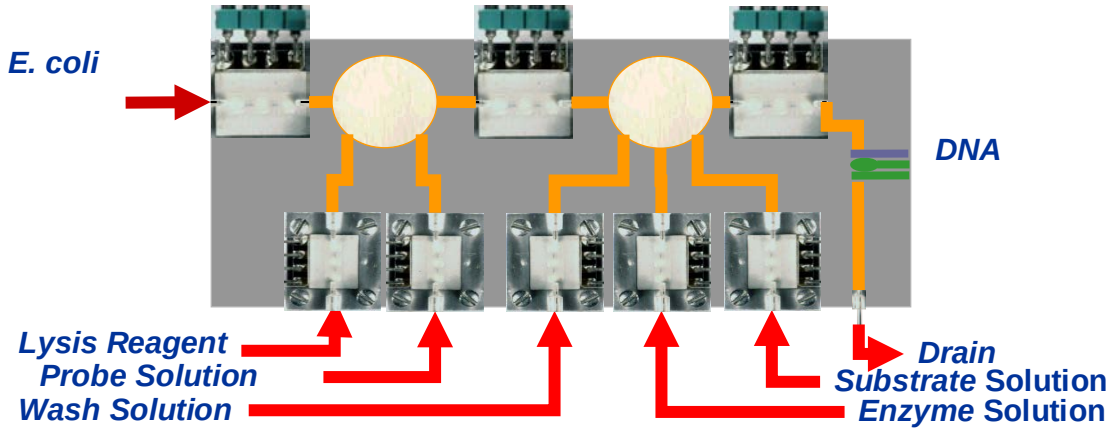

Figure 2: Integrated microfluidic lab-on-a-chip

The Stokes, or creeping, flow solution of the Navier-Stokes equations best describe microscale fluidics. In general, these highly viscous flows are well understood, and have been leveraged for such applications as capillary electrophoretic separations of biomolecules[2]. However, to achieve the vision of truly specific, sensitive lab-on-a-chip systems, further advances must be made to allow more robust manipulations of small volumes of fluid and the information rich biomolecules inside. Traditional surface and bulk micromachining has been used to develop a variety of mechanical valves and pumps. A typical valve or pump relies upon the deformation of a thin membrane to push or block fluid flow. To generate deflection of membranes, large forces are often required to overcome the high elasticity modulus of typical deposited thin films materials[3].

2.2 Hydrogel Valves

Simple, reliable, and reusable micro pumps and valves are key technology components of biodetection systems. To date, a wide variety of schemes have been demonstrated for both

passive and active valves on the microscale. Mechanical valves are typically fabricated from etched silicon and deposited thin films. Actuators have been driven by thermopneumatic, electrostatic, or magnetic fields. Despite the typical advantages of micromachining, these valves have not gained widespread use due to the high power requirements as these forces scale unfavorably with length. More recent work has expanded the range of actuator materials to polymers. These systems are developed to create easily manufacturable systems. A thorough description of crosslinked polymers in a solvent, known as hydrogels, is found in chapter 4. Here we will review valving designs based on hydrogel actuation.

David Beebe et al. were the first to develop micromachined hydrogel valves in 2000_4, shown in Figure 3. The main goal of this research was to develop a biomimetic self-regulating system based on pH. Microscale hydrogel was developed to reduce the response time of the gel, which is typically diffusion-limited. A step response of less than 10 seconds was observed for a cylinder 50 μm high and 100 μm in diameter.

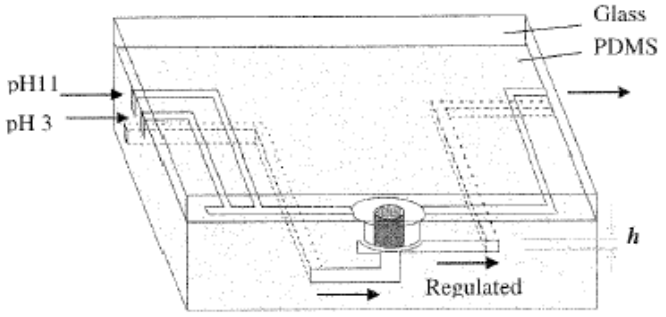

Figure 3: Self-regulating pH sensitive hydrogel valve

A combination of monomers and photoinitiator was flowed into a microchannel, and exposed through a mask. The monomers were a 1:4 molar ratio of acrylic acid and 2-hydroxyethyl methacrylate (HEMA) with a 1% addition of ethylene glycol dimethacrylate. Initiators such as Igracure 651 could be polymerized in as few as 20 seconds. The minimum resolvable feature size demonstrated with this technique was 25 μm, which was limited by the mask resolution.

The time constant of the gel's response to a change in pH was found to be proportional to the square of the dimension of these gel structures. A 10-second response was observed for a 100 μm-diameter cylindrical structure, but the gel was mechanically unstable. Hydrogels were noted to buckle if their lateral dimensions were less than their height. The solution to the buckling problem was to fabricate the hydrogels as toroidal structures around a post.

To demonstrate the valving function, solutions of varying pH were pumped at a flow rate of 0.15 mL/min through the microchannels. An array of hydrogel structures measuring 300 μm x 700 μm were used as valves. One formulation of the gel results in contraction in an acidic environment. At low pH values, the gel valves produced a pressure drop of 0.09 psi. When the gels were introduced to a basic solution, the pressure drop increased by a factor of eight. A different chemistry was used to create another gel that expanded in acidic environment. These two gel types were used to create a self-regulating system. At low pH, the valve to a basic buffer is opened, and at high pH, access to the acidic buffer is opened.

Subsequent research demonstrated the fabrication of biomimetic valves[5]. The biomemitic

feature of these valves is that they effectively prevent backflow at low pressures. This effect is achieved through the use of a bistrip hydrogel fabricated with both parallel and sequential photopolymerization. The first set of strips is fabricated to expand at high pH and shrink at low pH, with a phase transition at approximately 5. The solution is then washed away. Another set of hydrogel strips insensitive to pH are then polymerized adjacent to the first pair. This second set of hydrogel strips is used to anchor one end of the bistrip to the channel. When this bistrip is exposed to a pH of 8, the pH-sensitive strips swell while the insensitive strips remain the same length, effectively creating a check valve, as illustrated in Figure 4.

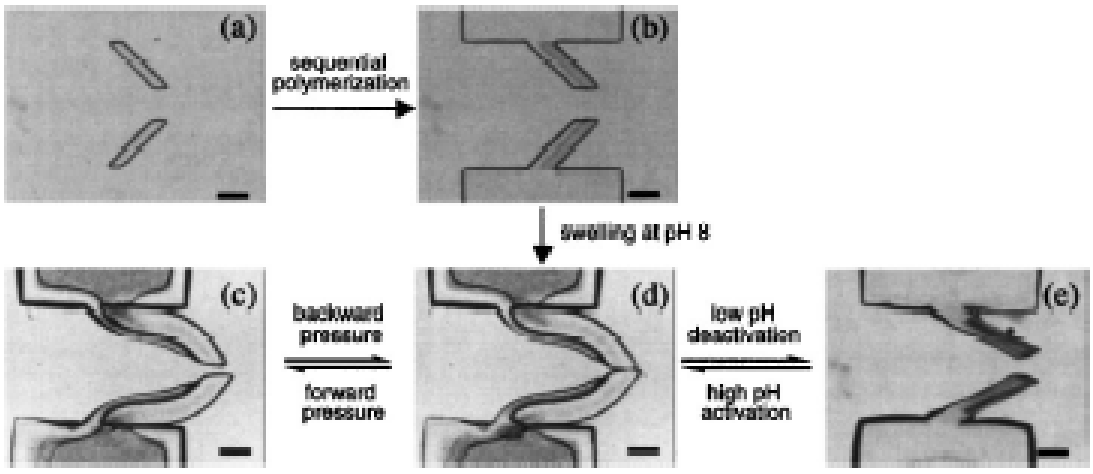

Figure 4: Microfabricated pH-sensitive hydrogel check valve

When the gel is contracted in an acidic solution of pH=3, the valve opens and allows flow in either direction. The forward flow rate for this valve was 140 μL/min at an applied pressure of 0.71 psi. The leakage rate in the reverse direction was 2.3 μL/min at the same pressure. At higher pressures, both forward flow and leakage increased significantly, due to the low modulus of elasticity of gel. At 1.56 psi, the forward flow rate was 390 μL/min, and the leakage rate was

20 μL/min.

2.3 Hydrogel Pumps

The low Reynolds regime that microfluidic circuits operate under requires different flow control mechanisms than macroscale fluidics. A wide array of pumping schemes has been developed, analogous to the thermal, electrostatic, magnetic actuation schemes developed for valves. In addition, electrophoretic and dielectrophoretic forces, electrothermal forces, and electrowetting are a subset of the other pumping forces that do not require displacement. However, lab-on-a-chip systems that utilize heterogeneous fluids, such as blood or sputum, may be subject to fouling when non-displacement based pumping methods are used. To date, research into polymer-based pumping schemes has not yielded as many useful systems as research into microvalves. A review of efforts in the field of hydrogel-based pumps indicates the success and limitations of current technologies.

The first use of N-isopropylacrylamide (NIPA) gels for a micropump was described by Suzuki in 2002[6]. This novel system was based on the concept of an "intelligent mosquito" and incorporated a sampling mechanism featuring the NIPA gel, a microscopic needle, and a micromachined glucose sensor. NIPA gel will be further described in subsequent sections, but the essential feature of this gel is that it experiences a discontinuous phase change when heat is applied. This phase change results in a release of water from the gel, resulting in a dramatic volume change that may be used for actuation.

The sampling mechanism shown in Figure 5 was formed on a silicon substrate with two etched chambers formed in the substrate. One of these chambers was used to contain the gel, and the other chamber was used to hold a reservoir of water. The gel-containing chamber contained a hole at the bottom covered by silicone rubber that interfaced with the microchannel used to conduct the sample fluid. The gel containing chamber measured 2 mm x 10 mm x 0.19 mm. The authors noted that transducing the volume change into a movement of the solution in a reversible manner is difficult since the change in the total volume of gel and solvent is negligible after the phase transition. In other words, the total volume of the gel in its hydrophilic state is approximately equal to the total volume of the collapsed gel and the water released from the gel. Therefore, the silicone rubber membrane was used to separate the hydrogel from the fluid to be pumped. When the gel was below the transition temperature, the gel would siphon water from the reservoir, swell, and cause the silicone membrane to press into the microchannel. When the hydrogel was raised above the transition temperature, the gel released water back into the reservoir, and the silicone rubber receded into the microchannel wall. The spring effect of the silicone rubber was used to push the liquid water from the gel back into the reservoir.

The volume transition from the hydrophilic state to the hydrophobic state occurred within 1 minute. The internal pressure of the gel was sufficient to deflect the 190 μm thick silicone rubber diaphragm into the microchannel. When the gel shrank, the elastic force of the rubber was sufficient to force the released water back into the reservoir. Step change between the hydrophobic state and hydrophilic state was used to measure the

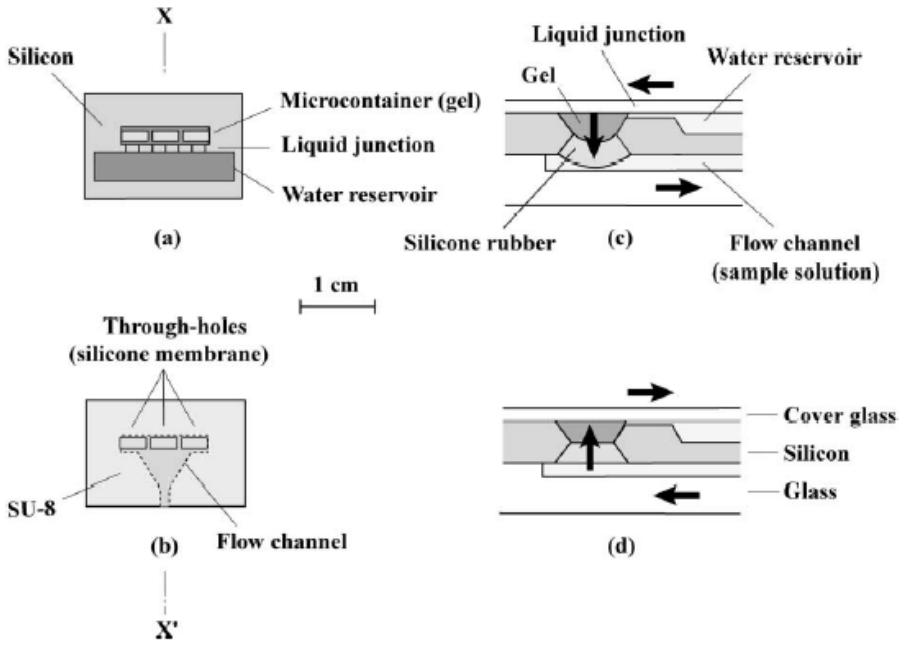

Figure 5: Thermally activated NIPA hydrogel pump

pumping effect. Each phase change resulted in the movement of 0.1 μL inside the adjacent microchannel. Although this method resulted in pumping, the time constant of the gel prohibited its use in a more useful system, such as a peristaltic pump. It would be difficult to extend this design to pump larger volumes of fluid.

2.4 Lasers for Sensing and Actuation

To generate truly useful μTAS (micro-Total Analysis Systems) for biological pathogen detection, simple, low cost methods of manufacturing these disposable chips must be developed. Therefore, it is undesirable to use incompatible methods for valving and pumping. In addition, the flow control techniques must be easily integrable with the sensor technology used to gather biological data. Therefore, some consideration must be given to the likely sensor technology.

Currently, most lab-on-a-chip systems utilize either electrochemical or optical sensors for DNA-based detection protocols. An optical sensor capable of detecting a single molecule of DNA via laser-induced fluorescence has been developed at UCLA[7] and is shown in Figure 6:

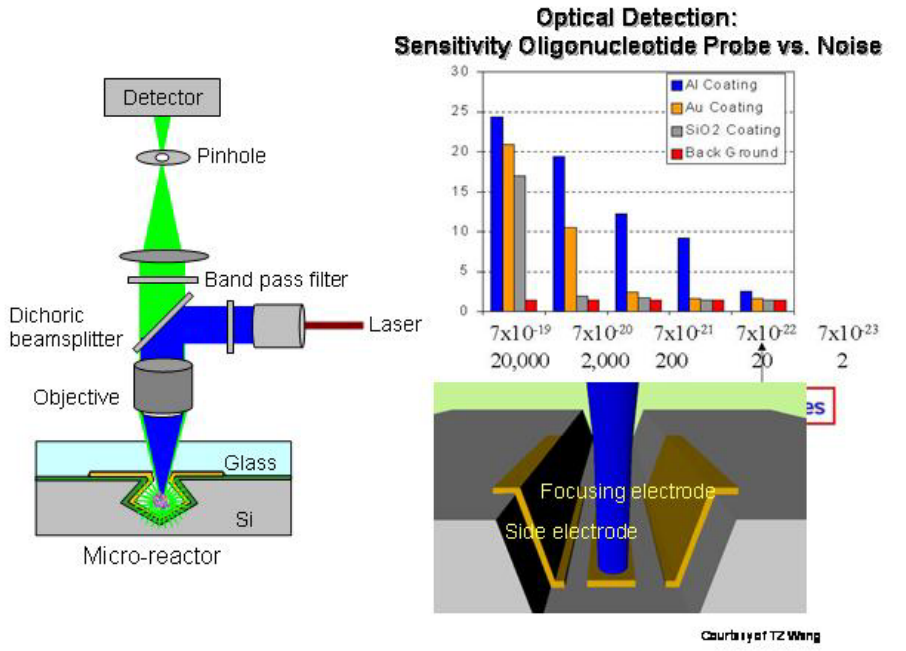

Figure 6: Optical DNA sensor for pathogen detection developed at UCLA

Optical sensors currently require an off-board laser, which limits portability and cost. For high-throughput bio-detection, micromachined disposable chips may be used with a detection station consisting of a laser, data acquisition hardware, and a computer. Since the high-powered laser is a suitable power source, it would be ideal to use the laser as an energy source for actuation.

Chapter 3

DEVLOPMENT OF RESPONSIVE HYDROGELS

3.1 Hydrogel Formulation

A polymer gel consists of a cross-linked network of polymers suspended in a solvent, as shown in Figure 7. The properties of the gel are dependent on the interplay between the polymers and solvent. The liquid suspends the polymer and prevents collapse. The polymer network retains the liquid and gives it form. Common examples of natural gels include the vitreous humor that fills the interior of the eye and the mucopolysaccharide gels that line the stomach and intestine. Research in this field expanded with the advent of poly (2-hydroxyethyl methacrylate) hydrogels used for contact lenses. Hydrogels are now used as drug delivery platforms, biosensors, and biomembranes. Tanaka pioneered research of responsive hydrogels as electrical, thermal, photonic, and pH-driven actuators[8].

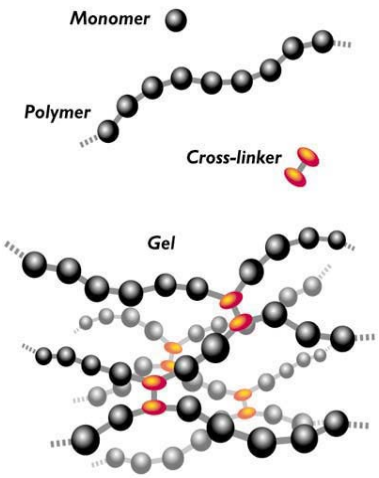

Figure 7: Essential features of a hydrogel

The main constituent of the network is the polymer backbone, which gives the hydrogel many of its unique properties. This backbone may either be a polymerized monomer or a block copolymer. The crosslinks of the gel may be either chemical or physical, and often determine the strength of the gel. Examples of physical cross links include entanglements or weak associations such as hydrogen bonds or Van der Waals interactions. Hydrogels are either neutral or ionic, depending on the ionization of their pendant groups. The ratio of polymer to solvent by weight may vary from 1:5 to 1:1000.

Three properties are used to characterize hydrogels: polymer volume fraction in the swollen state, $\upsilon_{2,s}$, number average molecular weight between cross links, $\overline{M_c}$,and the correlation length, also known as network mesh (or pore) size ξ. The polymer volume fraction is the ratio of the volume of polymer Vp, to the volume of the swollen gel, Vgel. The number average molecular weight between cross-links, $\overline{M_c}$, is the molecular weight of the repeating unit of the polymer divided by twice the degree of cross-linking. The correlation length is a measure of the distance between cross links.

Polymers may exist is solid, liquid, or gaseous form, depending on the temperature, volume, and pressure of the system. The mechanical properties of the polymer are dependent on the phase, and a phase diagram yields useful information about how molecules interact. Many polymers have the unique property of exhibiting a phase transition. Drastic changes in the state of the polymer can be brought about by small changes in external conditions. These include

temperature, pH, chemical agents, mechanical forces, solvents, or electric fields. For hydrogels, this may result in a change in volume by as much as a factor of 500. The volume transition results from the balance between three osmotic pressures acting on the polymer network: positive pressure of counterions, negative pressure due to polymer-polymer affinity, and the elasticity of the network itself. The cumulative effect of these three pressures determines the equilibrium volume. A moderate change in one of these factors creates pressure that results in a new equilibrium volume.

3.2 Theoretical mechanism for the absorption and release of water by N-isopropylacrylasmide (NIPA)

NIPA $(C_6H_{11}NO)_n$ can exist in both crystalline and amorphous forms, and has a glass transition temperature of 134^0C. The gel formed from NIPA has an opaque microporous structure, formed from fine fibers less than 5 μm in diameter. It exhibits a reversible affinity for water based on temperature and forms the main constituent of our gels. NIPA gels undergo a phase transition as the local polymer network is heated. This transition may be either continuous with temperature or discontinuous, depending on the solvent used and presence of a comonomer. Our formulation of the NIPA gel can discontinuously contract or expand volumetrically 50% or more at a temperature of 33^0C. This process is repeatable and reversible.

The water release and absorption mechanism of NIPA gels is still poorly understood. According to Tanaka, the existence of multiple phases for gels is a result of competing forces within the gel such as mixing enthalpy and entropy, rubber elasticity, columbic interactions between charged

groups, and between charged groups and counter ions. In thermodynamic terms, these interactions are scalar quantities. Therefore, the volume of the gel is determined by the net sum of these interactions' contribution to free energy. Tanaka suggests that the phenomena may be a result of a vector addition, rather than a scalar addition, since some of these interactions may be direction dependent. A good example would be the nature of hydrogen bonding to align molecules and induce further bonding.

This suggests a simple model for the rapid nature of the phase transition. If the hydrogel in its hydrophilic state has many layers of water surrounding individual NIPA strands, a slight perturbation to favor polymer-polymer interaction will destroy the water layering and will transmit rapidly along the polymer chain. The release of water increases the opportunities for polymer-polymer interaction, so this becomes a self-accelerating process. Like a zipper becoming unzipped, the layers of water pull away.

3.3 Formation of NIPA hydrogels

The basic NIPA gel is formed by free radical polymerization in water at ~4 deg C. A recipe for eliminating inhibitors from NIPA is given in Appendix A. Various recipes for creating basic NIPA gel are given in Appendix B. The gel chemistry for the basic formula is shown in Figure 8:

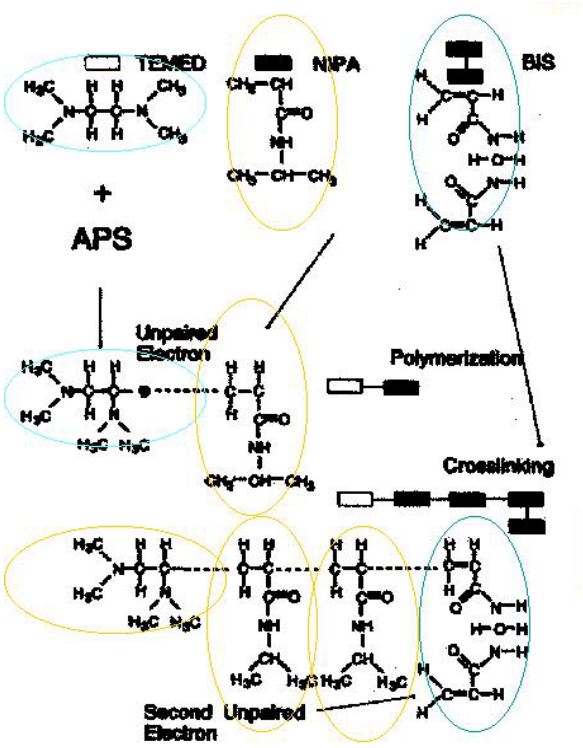

Figure 8: Essential formulation of NIPA hydrogel

The main constituent is the NIPA monomer, which links together to form a chain. The long NIPA chains are converted into a web of interlocking chains with the addition of bisacrylamide (BIS). BIS has two functionalized sites and acts as a branch point. Increasing the amount of BIS in the gel produces a denser, more tightly linked network. This has the effect of increasing the mechanical strength of the hydrogel, but the volume transition becomes more continuous over a range of temperatures. In effect, the swelling ratio and stroke length of the gel transition is reduced. For a disposable microvalve, a discontinuous response is desired. Therefore, the amount of BIS must be carefully tailored to trade off these two requirements.

The final two chemicals, ammonium persulphate (APS) and tertramethyl ethylene diamine (TEMED) initiate polymerization and the gelation process. TEMED, the accelerator, and APS,

the initiator, react to produce one unpaired valence electron[13]. This electron is transferred to a NIPA monomer, allowing it to bind to subsequent monomers and form a polymer. Reducing the amount of APS reduces the number of initiation points, and results in longer NIPA chains. This has the effect of making the gel more flexible. On the other hand, an insufficient amount of APS will result in incomplete polymerization and wasted monomers that serve no mechanical function. Increased amounts of APS will result in shorter chains and will also reduce the total gelation time. Oxygen has been identified as absorbing the unpaired electron and quickly terminating polymerization. This was been addressed by forming the gel in a nitrogen atmosphere. The inert nature of nitrogen allows the free radical to continue polymerization indefinitely.

3.4 Optical actuation of NIPA gel

Tanaka and Suzuki[14] first described the light responsive version of NIPA hydrogels. The NIPA gel was identical to the basic gel formula with the addition of a light sensitive chromophore, trisodium salt of copper chlorophyllin. The light is converted to heat by the dye, and the polymer backbone switches from a hydrophilic state to a hydrophobic state. This process is reversible. Other optically responding polymers have been developed, but rarely exhibit this magnitude of response[15].

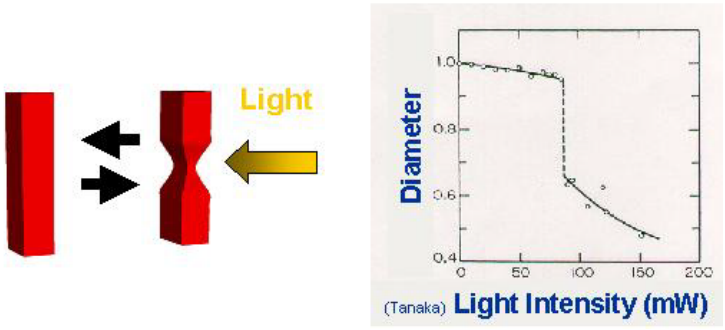

Figure 9: Light induced hydrogel phase transition

Figure 9 shows the published volume transition of this gel inside a capillary.

In their experiments, Tanaka and Suzuki fabricated the gel inside glass capillaries with 100 μm inner diameter. An argon laser at 488-nm was focused to a 20 μm spot size. The power of the laser was varied from 0 to 150 mW. At an intensity of 120 mW the gel showed a discontinuous volume transition at 31.5^0C. This effect was observed at both a pH of 11.9 and a pH of 5.8. The researchers noted that phase transition induced by light resulted in a more discontinuous shift and the temperature of transition was lowered. Tanaka estimated that a 1 μm diameter gel would respond in 5 ms.

Similar experiments were conducted to learn about the function of the gel. The most difficult aspect of the experiments to recreate was the formation of the gel itself. Whenever a minor concentration of chlorophyllin as added to the pre-gel mix, gelation would invariably fail. This is understandable because the chlorophyllin is an electron scavenger, and therefore will act quickly to terminate free radical polymerization. The solution to this problem was to add the dye after gelation. Once this was resolved, our results were fairly similar to Tanaka's.

The gel was pumped into a glass microcapillary with a 1.5 mm inner diameter and activated with an Argon laser at 488nm. The gel began to respond at 40 mW of output power. The response was more dramatic at 60mW.

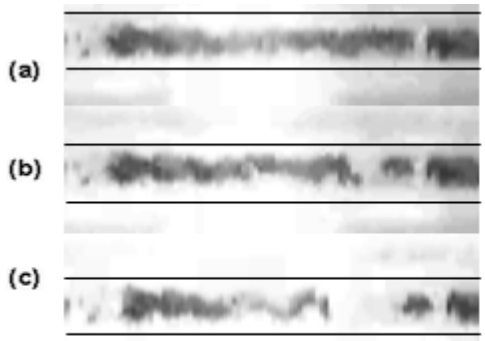

Collapse of gel; Argon laser at 60 mW

(a) t=0sec (b) t=18sec (c) t=27 sec

Figure 10: Collapse of hydrogel in response to laser light.

This is shown in Figure 10. The light black lines are the outline of the glass capillary. The dark indistinct regions are region where the chlorophyllin is very dense. The green bars represent the beginning and ending of a subsection of gel. The power requirement was notably less than that shown by Tanaka. This may have been due to the higher concentration of chlorophyllin dye in our gel.

3.5 Characterization of Dye Bond

In our experiments, the light-sensitive dye used in published research, chlorophyllin, consistently inhibited gelation. This problem was been resolved by chemiabsorbing the dye post-gelation. These experiments lead us to more carefully consider the type of bonding between the dye and the polymer network. We used differential scanning calorimetry to determine the nature of the bond between the dye and the gel as shown in Figure 11 and 12.

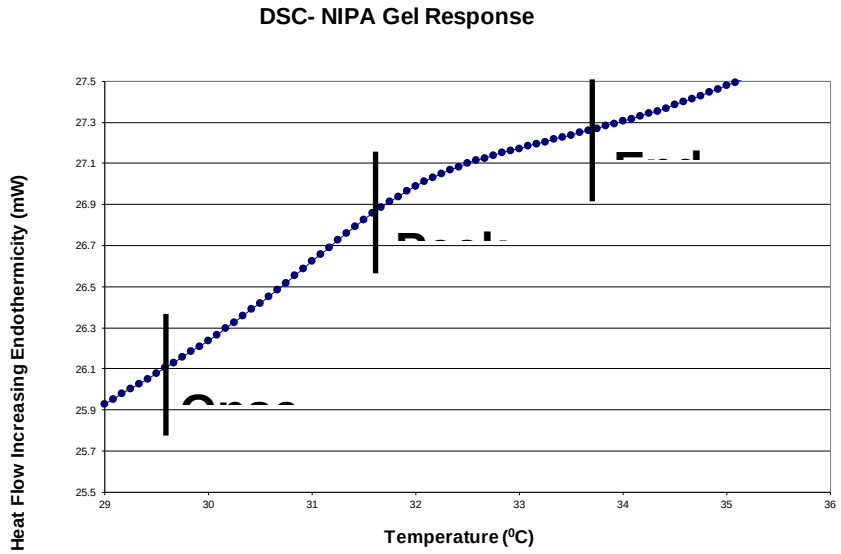

Figure 11. Differential scanning calorimetry of NIPA gels without dye

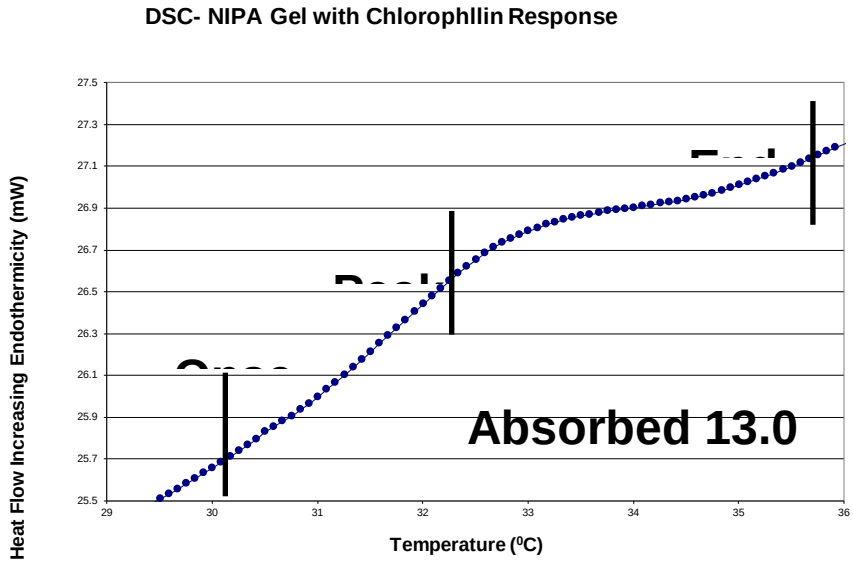

Figure 12. Differential scanning calorimetry of NIPA gels with chlorophyllin dye

The presence or absence of dye produces no appreciable change in the lower critical solution temperature. Therefore, the bonds between the dye and gel are weak, possibly van der Waals forces. This suggests a wide array of dyes may be introduced to NIPA gels via chemiabsorption. NIPA hydrogels have been fabricated with several common dyes to tailor mechanical actuation to the wavelength of the incident light. Chlorophyllin, coumarin 6, and rhodamine 123 have all been demonstrated. The specific absorbance spectra of the dyes allow different gels to be triggered by changing the wavelength of light as demonstrated in Figure 13.

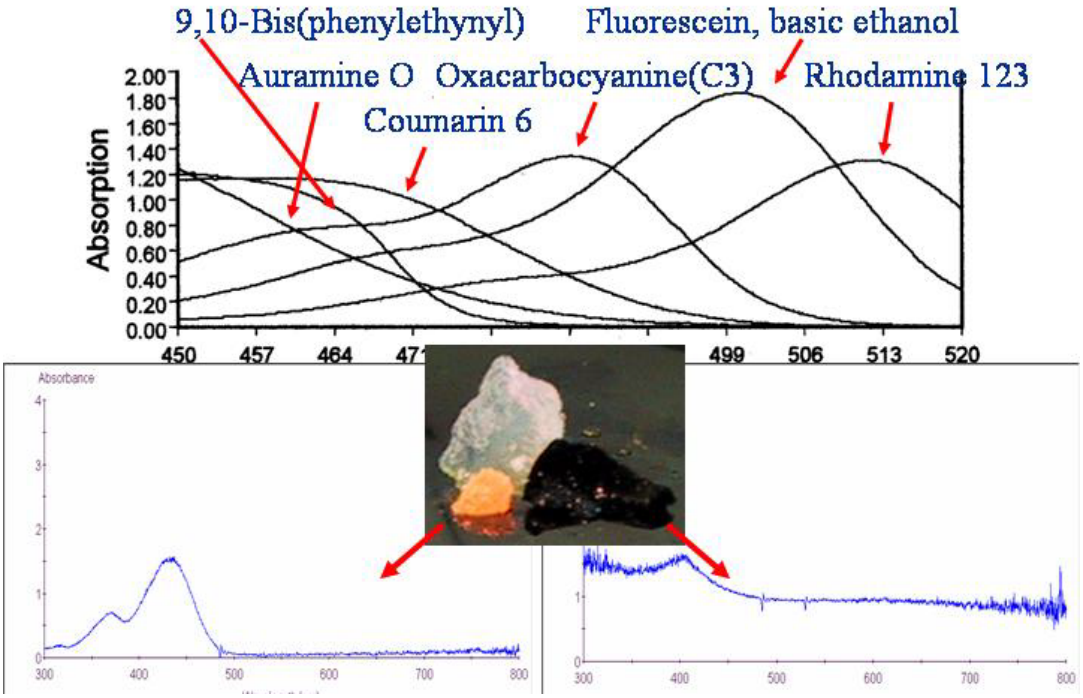

Figure 13: Novel light-sensitive gels and their absorbance spectra

This is the first time that hydrogels responsive to light have been tailored to specific wavelengths.

Chapter 4

HYDROGEL PHYSICS

Since these hydrogels are ultimately to be used in valving and pumping mechanisms, a model of the dynamic behavior of the hydrogel under an applied load and a method to gauge the gel's efficiency must be developed.

There are a number of analytical models used to predict the structure of biomaterials and to aid in the understanding of its structure at the molecular level. There are three models used for examining network structure formation: kinetic models, statistical models, and Monte Carlo simulations. Kinetic models consist of a set of differential equations representing the mass balance on the species. These equations yield the properties of the gel such as average molecular weight. Zhu et al. developed detailed models to examine crosslinking and cyclization in network formation[16]. The kinetic models determine properties of the system based on the continuum assumption. Statistical and Monte Carlo models have been developed to provide more insight into the network formation process and the local variations that occur.

4.1 Pressure within Hydrogel During Phase Transition

Nonideal thermodynamic frameworks can be used to describe the swelling and shrinking behavior of hydrogels. Volume-phase transitions were predicted in 1967 and the first experimental confirmation occurred in the late 1970's[17]. At particular environmental conditions, infinitesimal changes in the balance of intermolecular interactions, electrical charges, and

$$\Pi = \Pi_{poly-poly} + \Pi_{elastic} + \Pi_{ion}$$

hydrostatic pressure that comprise the osmotic pressure may result in a volume-phase transition. Positive osmotic pressure swells the gel, and negative pressure causes the gel to shrink. The three components of osmotic pressure are rubber elasticity, polymer-polymer affinity, and hydrogen ion pressure[18]:

Rubber elasticity is a thermally dependent, bi-directional force that opposes changes in the gel shape away from its equilibrium state. This may be modeled as a series of interconnected springs.

Polymer-polymer affinity encompasses four different interactions, including attractive and repulsive forces between polymer strands or between a strand and the ambient solvent. The van der Waals force is present between molecules in a non-polar solvent. Hydrophobic forces between the polymer chain and adjacent water molecules cause the water molecules to form highly ordered structures, resulting in a local reduction of entropy and enthalpy. Hydrogen bonding occurs between polymer stands. Finally, electrostatic interactions are the product of charges on the polymer chains. If the network has a net charge, such as NIPA does, counter ions position themselves near the chains. The concentration of counterions inside and outside the gel results in osmotic pressure.

Hydrogen ion pressure is similar to the osmotic pressure produced by the counterion balance. This additional pressure results from the motion of the ions within the gel.

A substantial body of work has been developed by chemists to describe pressure in polymer solutions and networks. This should be acknowledged in any discussion of gel systems. In general, the Flory-Huggins equation of state is the most widely used equilibrium model of pressure in a gel network[19]. This equation is derived from a Gibbs free energy formulation.

$$\frac{1}{T} = \frac{\Delta S}{\Delta H} + \frac{k}{\Delta \mathrm{H}}\left(\frac{v_1 \upsilon_e}{N\phi^2}\left[(2f+1)\left(\frac{\phi}{\phi_0}\right) - 2\left(\frac{\phi}{\phi_0}\right)^{1/3} \right] - \frac{2}{\phi} - \frac{2\ln(1-\phi)}{\phi^2} \right)$$

This highly nonlinear equation usually requires numerical solutions. For the family of gels characterized by Flory interaction parameters and frictional coefficients similar to NIPA, the resulting P-V diagram is of the same general form as a van der Waals' material. For Van der Waals' material, an increase in pressure results in a decrease in volume except during phase changes. Gels experience a similar plateau during transition from a hydrophobic state to a hydrophilic state. The benefit of the Flory-Huggins model is that it is not a mathematical analogy. Rather, this model predicts the gel's osmotic pressure from first principles and predicts when the gel's P-V relationship deviates from this behavior. Unfortunately, the Flory-Huggins model is poorly suited to include terms for work done by or on the gel and can't be used to evaluate efficiency, and is therefore inappropriate for use in a valve control scheme. Ultimately, a state space model would be useful to design the hydrogel valve and predict its behavior under various load conditions.

4.2 Swelling Behavior of Gel

Researchers' progress in kinetic models for gel behavior has lagged the steady state models. Current models, largely developed by Toiyoichi Tanaka, relate the volume change in a gel to the

diffusion of the network in the solvent[8]. Previous efforts described the gel's motion as limited by the diffusion of water into the gel. The size and shape of the gel and the collective diffusion coefficient:

$$\boldsymbol{D = \frac{k}{f}}$$

dictate the rate of network motion relative to the solvent. K is the elastic modulus of the polymer network and f is the frictional coefficient, which are, in turn, dependent on temperature, ionic content, and volume of the gel. Tanaka and Fillmore demonstrated that the equation of motion for a swelling gel is given by:

$$\frac{\partial u}{\partial t} = \nabla \bullet \sigma / f$$

$$\sigma_{ik} = K\nabla \bullet u\delta_{ik} + 2\mu\left[\frac{1}{2}\left(\frac{\partial u_k}{\partial x_i} + \frac{\partial u_i}{\partial x_k}\right) - \frac{1}{3}\nabla \bullet u\delta_{ik}\right]$$

u(r,t) – the displacement vector of a point in the network after it is fully swollen

f – the friction coefficient between the network and the fluid medium

σ – stress tensor

K – bulk modulus of the polymer network

μ – shear modulus of the polymer network

The first term in the stress tensor represents the stress produced by a volume change, and the second term is the stress caused by shear deformation. Tanaka and Fillmore simplified the analysis for a spherical gel. The spherical symmetry simplifies the equation to:

$$\frac{\partial u}{\partial t} = \left(\frac{K + 4\mu}{3f}\right)\frac{\partial}{\partial r}\left\{\frac{1}{r^2}\left[\frac{\partial}{\partial r}\left(r^2 u\right)\right]\right\}$$

Using this equation, initial conditions and boundary conditions derived from the gel stress states before and after swelling, a solution may be obtained:

$$u(r,t) = \frac{6\Delta a_o}{\pi^2}\sum_{n=1}^{\infty}\frac{e^{\frac{-n^2 t}{\tau}}}{n^2}$$

where:

a – final radius of gel sphere in equilibrium with the surrounding fluid

Δa_0 - total increase in the radius of the sphere during swelling process

and

$$\tau \equiv \frac{a^2}{\pi^2 D_c}$$

Thus, the time constant for swelling is proportional to the square of the radius of the gel. One of the more interesting aspects of gel kinetics is this dependence on shape. Experiments have validated that the kinetics are usually a function of the critical, or smallest, dimension of the gel. The volume phase transition is fastest along this dimension, since it is a diffusion-driven process. As soon as the gel changes in one dimension, the shearing due to the interconnection to the network causes the rest of the polymer to follow suit. The end result is isotropic swelling or shrinking of the gel when unloaded and uniformly cross-linked. Therefore, for a hydrogel valve with rapid response, a long, thin structure is ideal. Similar analysis as demonstrated above has generated a time constant applicable to non-spherical volume-phase transitions[20]:

$$\tau = \frac{L^2}{\pi^2 D}$$

Where L is the critical dimension. This confirms the utility of the "long, thin" gel design. It is predicted that gels with critical dimensions measuring tens of microns will respond within seconds. Our experimental results of gels with critical dimensions in the 100 μm-1 mm agree with these estimates. Initial hydrogel actuators typically took minutes to respond to stimulus, since the response rate is proportional to the square of the smallest length dimension of the gel.

Independent of the relation to size, the swelling behavior was governed by two apparent time constants. The gel initially swells quite slowly. As the network expands and the polymer-polymer interactions decrease, another time constant comes into play and the gel swells more rapidly. In Matsuo's and Tanaka's work[21], they measured the time constants of spherical NIPA gels ~200 um in radius. In these experiments, spherical gels were maintained in baths below the phase transition temperature, and then were introduced to baths below the transition temperature while their motion was recorded. Their results consistently showed their gels required roughly 200 seconds to fully expand. This number is relevant to our experiments because our gel valves are comparable in size.

4.3 Shrinking Behavior of Gel

According to Matsuo and Tanaka, the process of gel shrinking is more complicated than the swelling process. A spherical gel will maintain its shape as it decreases to 70%-90% of its original size. After that, the gel stops shrinking for a period of time. This occurs because the gel initially shrinks at the point of heat transfer-at the surface. Thus, a layer of dense, collapsed

network is formed at the gel surface, inhibiting fluid transfer from the interior to the outside of the gel. During this period, the density of the gel and the osmotic pressure within the gel vary as a function of radius due to the diffusion process. During the plateau phase, the osmotic pressure inside the gel exerts force on the impermeable gel layer which is trying to shrink. Eventually the pressure balances and the fluid from inside the gel is released in a second shrinking stage. In Matsuo's and Tanaka's work, they measured the three time constants of the first and second shrink phases as well as the plateau. All three time constants are strongly dependent on the final temperature of the gel. If the final temp of the gel is just above the phase transition temperature, the second shrinking phase can last as long as 10 minutes! This slowing down effect near the transition temperature was also noted for the swelling process. For final temperatures 5^0C or more above the transition temperature, the first shrink takes a second or less, the plateau phase lasts 10 seconds or less, and the final phase takes 30 seconds or less. According to the transport derivation, the time constant should vary as the square of the radius of the gel. Experimentally, the value of the exponent for swelling is 1.8, and 1.6 for shrinking. More relevant to the proposed application, the overall time constant for swelling is larger than the shrinking time constant. This difference is again strongly influenced by whether the final temperature is close to the transition temperature. In cases where the final temperature is well beyond this point, the swelling time may be as much as an order of magnitude greater than the shrinking time. Thus, for a 200 μm radius gel, the time to become fully hydrophobic was approximately 20 seconds. These times are similar to the results demonstrated with the valves we've fabricated.

Note that the equations derived for gel swelling are applicable to gel shrinking as well with two important points. First, the analysis presumes friction, f, is constant. This does not hold during the plateau phase, when the density of the outer radius of the gel is greater than then inner core of the gel. Thus, the plateau phase is not adequately represented by this model. For gels with short plateau phases, such as the NIPA gels we used with critical dimensions below 500 μm, this does not prohibit the use of these expressions for both swelling and shrinking. The second point is that both the friction factor and elastic modulus of the polymer are different between the swelling and shrinking case. In the shrinking case the friction is between the free standing polymer strands and bulk water. In the swelling case, polymer-polymer interactions impede the free flow of water. Likewise, the polymer-polymer interactions impact the elastic modulus of the network. Thus there are significantly different time constants between these two types of motion.

4.4 Dynamic Model of Gel

A model of the gel's response to incident light, namely radiative heat transfer from the laser to the gel, is helpful in developing the gel valve. This analysis will be conducted separately, as the focus of this section is the behavior of the gel. The goal of the dynamic gel actuator model is to reasonably predict mechanical behavior of the gel in a manner that is easily solvable and can be applied to different applications. A linear model would be ideal for stability, performance analysis, and control design.

As discussed in the background section, the kinetics of the gel system are governed by the components of osmotic pressure. These, in turn, impact the diffusion of the solvent through the

network polymer. According to this description, the radius of the gel changes rapidly for times smaller than τ and follows a single exponential profile afterwards[22]. The diffusion coefficient, Dc, and the critical dimension of the gel characterize this diffusion process.

$$u(r,t) = \frac{6\Delta a_o}{\pi^2}\sum_{n=1}^{\infty}\frac{e^{\frac{-n^2 t}{\tau}}}{n^2}; \tau = \frac{L^2}{\pi^2 D}$$

Note that the exponential, which dominates the sphere's motion, is a function of the diffusion coefficient and the longest dimension of the gel. This two time-scale property of the solution will be the basis for a second order linear approximation for the diffusion dynamics under a small volume change.

For a given change in temperature, we desire the output force of the gel system. This is a two step process. First, the temperature varies with the osmotic pressure during a volume phase transition. This will be referred to as the active gel unit of the model. Then the force of the osmotic pressure and any external load present is applied to the passive model of the gel system. This passive gel unit represents the mechanical linkage of the gel and its load. Note that the final position of the gel, y, is dependent on the external load, F2. This is illustrated in Figure 16:

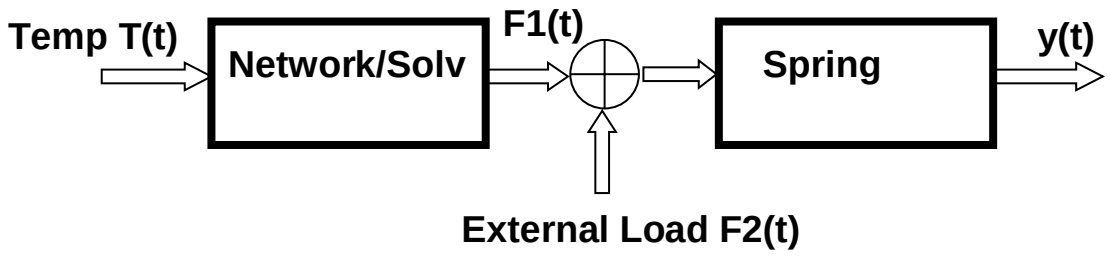

Figure 16: Active and passive components of gel model

In a microscale application, an important part of the external load is the friction between the gel and the substrate it rests on. The dynamics of the passive component are generally faster than the active component since the polymer has very short shear time constants.

Two variables, the diffusion coefficient D_c, and the critical dimension, a, characterize the simplified spherical gel equation. In all observed behavior of gels, the system is clearly overdamped. There is no oscillation indicative of underdamping. The simplest way to describe this overdamped second order system is with a two-pole model.

$$\frac{F_1(s)}{T(s)} = \frac{a}{s^2 + bs + c} = \frac{a}{(\tau_1 s + 1)(\tau_2 s + 1)}$$

The two time constants govern the decay times of the exponentials. Unfortunately, two degrees of freedom are insufficient to match the experimental results of a gel's volume change in response to a step change in temperature. Since the time constants are different by at least by an order of magnitude, there will be a large separation between the poles of this system. When there is a large distance between poles, the fast pole has a negligible impact on the response to a step input. Therefore, the system approaches a first order system. However, this first order behavior does not match the fast response of experimental results. Recall that for the case of shrinking, the initial motion is impeded by a plateau phase. For expansion, the diffusion of the gel network is dominated by the diffusion coefficient, but only after the polymer-polymer interactions have been surpassed. The minimum order system that demonstrates this behavior is a second order system with a finite zero:

$$\frac{F_1(s)}{T(s)} = \frac{ds+a}{s^2+bs+c} = \frac{A}{s} + \frac{B}{s-s_1} + \frac{C}{s-s_2} = \frac{a}{ss_1s_2} + \frac{ds_1+a}{s_1(s-s_1)(s_1-s_2)} + \frac{ds_2+a}{s_2(s-s_2)(s_2-s_1)}$$

where s1 and s2 are the solutions of the quadratic equation. The expression has been expanded by the method of partial fractions to show the influence of each term. The diffusion pressure that is the output of the active gel unit is the same whether triggered by a change in temperature or external tension on the gel. External tension on the gel is expressed as the external load, F2. Therefore, the relationship between the F1 and F2 is given by:

$$\frac{F_1(s)}{F_2(s)} = \frac{ms+n}{s^2+bs+c}$$

Finally the multiple-input, single-output active gel unit can be reduced to a state space formulation:

$$\begin{bmatrix} \dot{x} \\ \dot{F}_1 \end{bmatrix} = \begin{bmatrix} 0 & -c \\ 1 & -b \end{bmatrix} * \begin{bmatrix} x \\ F_1 \end{bmatrix} + \begin{bmatrix} a & m \\ d & n \end{bmatrix} * \begin{bmatrix} T \\ F_2 \end{bmatrix}$$

The dynamics of the passive gel unit are much simpler, since they are driven by the elastic nature of the polymer network. The spring coefficient depends on both the elasticity of the individual polymer strands as well as the network density. Since the network density changes as the gel expands or contracts, the spring constant will also. Therefore, the passive gel unit will most likely exhibit oscillatory behavior. On a practical note, the viscous damping inherent in the active gel unit effectively negates this proposed oscillation.

The transfer function for the internal force F_1 and the output y(t) is:

$$\frac{Y(s)}{F_1(s)} = \frac{1}{Ms^2 + Bs + K}$$

The same transfer function applies to F_2 and y(t):

$$\frac{Y(s)}{F_2(s)} = \frac{1}{Ms^2 + Bs + K}$$

The state space model for the passive gel unit is:

$$\begin{bmatrix} \dot{y} \\ \dot{v} \end{bmatrix} = \begin{bmatrix} 0 & 1 \\ -\frac{k}{M} & -\frac{B}{M} \end{bmatrix} * \begin{bmatrix} y \\ v \end{bmatrix} + \begin{bmatrix} 0 & 0 \\ -\frac{1}{M} & -\frac{1}{M} \end{bmatrix} * \begin{bmatrix} F_1 \\ F_2 \end{bmatrix}$$

Finally the active gel unit and passive gel unit are combined to create a complete linear model of the gel's behavior under an external mechanical load and an external temperature source:

$$\begin{bmatrix} \dot{x} \\ \dot{F}_1 \\ \dot{y} \\ \dot{v} \end{bmatrix} = \begin{bmatrix} 0 & -c & 0 & 0 \\ 1 & -b & 0 & 0 \\ 0 & 0 & 0 & 1 \\ 0 & \frac{1}{M} & -\frac{k}{M} & -\frac{B}{M} \end{bmatrix} \begin{bmatrix} x \\ F_1 \\ y \\ v \end{bmatrix} + \begin{bmatrix} a & m \\ d & n \\ 0 & 0 \\ 0 & -\frac{1}{M} \end{bmatrix} \begin{bmatrix} T \\ F_2 \end{bmatrix}$$

The overall model is fourth order, with both the active and passive units each contributing two poles. Having completed the task of deriving expressions for the efficiency of the gel engine and a state space model of the gel dynamics, what useful information may be obtained? The main use of this model is that experimental determination of the diffusion coefficient, length of the gel, elastic modulus, and the network density, allows us to predict the displacement of the gel, y(t), for a given change in temperature T(t).

Examining the transfer matrix of the dynamic model, the nonzero term in the fourth row, second column of the state dynamics matrix represents the series connection between the force from the diffusion process to the mechanical linkage. The sub-matrix, A, yields eigenvalues describing the relation between the force F1 and temperature T.

$$A_D = \begin{bmatrix} 0 & -c \\ 1 & -b \end{bmatrix}$$

The eigenvalues indicate that this process is much slower than the dynamics of the mechanical system, the passive gel unit. In other words, the diffusion coefficient and the critical length dimension of the gel dominate the gel's response, rather than the elastic modulus or network (i.e. crosslink) density.

To critically evaluate the accuracy of this dynamic model requires experimental data currently unavailable, namely the diffusion coefficient. However, a few points may be made. As noted earlier, the shrinking action of the gel is much faster than the swelling. Therefore, two values of the diffusion coefficient must be used to reflect the difference between swelling and shrinking motion. The second order transfer function was utilized to match the time constant of the gel to previous research, so this aspect of the model may be judicious. It is likely that the motion of the gel will deviate from the model when the gel undergoes more non-linear behavior. This is anticipated to occur at the limits of the range of motion of the gel, namely fully tumescent and fully dehydrated gel.

4.5 Efficiency of a Gel-based Engine

Now that we have a model to predict the gel's motion, we can derive a figure of merit to evaluate the utility of using hydrogels for micromachines by estimating the efficiency of the conversion of light energy to mechanical work on the fluid. The overall efficiency is dependent on the absorbance of incident light and the thermodynamic transfer to work. The quantum efficiency is a measure of the dye's ability to absorb incident light. As stated previously, this quantity is tailored through the use of different dyes. To estimate the thermodynamic efficiency, we'll consider the gel as a heat engine.

We may evaluate the gel efficiency as the efficiency of a heat engine operating between two thermal reservoirs if the condition of quasi-static equilibrium is applicable. Quasi static equilibrium conditions exist when the volume change is slow enough to ensure reversibility without dissipation. As suggested in the previous sections, the reversibility requirement is more easily met in the swelling condition than the shrinking condition, due to thin collapsed layer that form at the surface. However, the applicability of quasi-static equilibrium to both swelling and shrinking is borne out by experimentation[23]. For the NIPA gel, temperatures of 24^0C and 45^0C are suitable for the reservoirs, since these are the upper and lower limit of the volume phase transition for the basic gel formula. For any cycle, efficiency is defined as:

$$\eta = \frac{W_H + W_L}{Q_H}$$

Using the suggested thermal reservoir temperatures, the thermodynamic efficiency has an upper limit of 10%-not too good. There is an important caveat to this expression. The efficiency formulation for an engine assumes that positive (useful) work is done during expansion, and

negative work is done during contraction. The elastic nature of gel allows positive work to be done during both expansion and contraction. This can be easily envisioned in a simple gel-based pumping mechanism. Therefore, the efficiency definition will depend on the application of the gel. We intend to use the volume-phase transition of the gel to drive the valving or pumping motion. This phase transition involves the transfer of energy that may be stored in the gel. With this in mind, a more general expression for the thermodynamic efficiency of a hydrogel can be derived.

A temperature change unbalances the osmotic pressure within the NIPA gel and drives it to a new volume where the internal and external pressures will match. Since the gel will be exercised along the volume phase transition, the gel will expand along one temperature curve on the P-V diagram. As the gel is cooled, it is transferred to another temperature line, where contraction can occur. This process is shown in Figure 17 and 18.

The cycle is comprised of four distinct parts. From equilibrium point 1 to 2, the gel engine is

$$Q = m_s \int_{T_L}^{T_H} c_s(T)dt + m_n \int_{T_L}^{T_H} c_n(T)dt > 0$$

heated isochorically. In other words, the gel shifts to a new temperature curve but has no time to change volume. The flow of heat is:

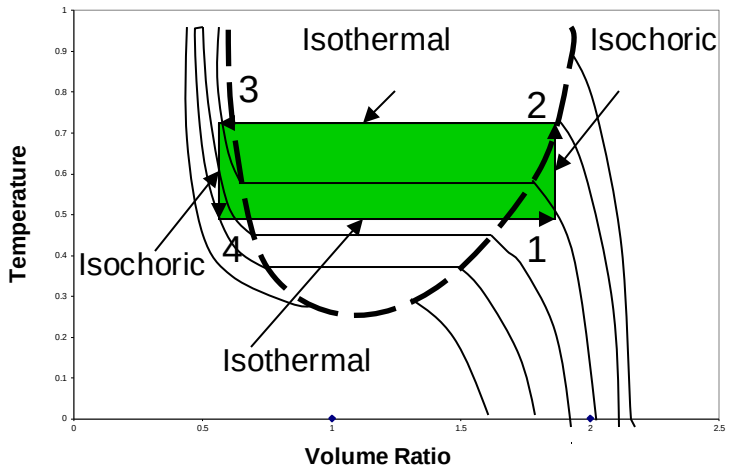

Figure 17: T-V diagram for a gel-based engine

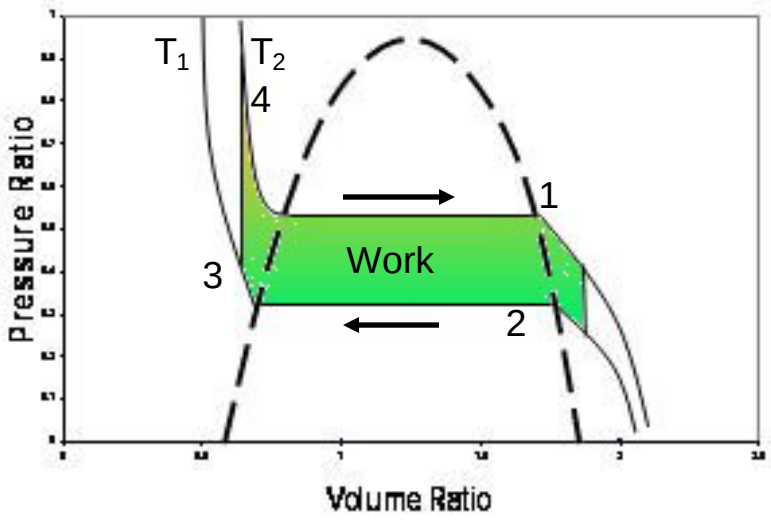

Figure 18: P-V diagram for a gel-based engine

The variables m_s and c_s are the mass and specific heat of the solvent, and m_n and c_n are the mass and specific heat of the polymer. No work is done during this step.

Form point 2 to 3, the gel engine undergoes isothermal contraction. At this point the gel has shifted to a new temperature curve, where the osmotic pressure is no longer in equilibrium. As the volume decreases, the internal pressure increases until the gel reaches a new equilibrium point on the other end of the volume phase transition. The total heat transfer in this step is the latent heat transfer in the state transition as well as the heat associated with the volume change:

$$\boldsymbol{Q_{ITC} = Q_{HL} + Q_{HW}}$$

Where Q_{HL} is the latent heat of changing the state, and Q_{HW} is the energy that is converted to work through volume change. The work for this segment of the cycle is:

$$W = \int_{V_2}^{V_1} \pi(V) dV$$

Since heat is transferred into the gel system, we may assume that the entropy of the system increases as well. However, the volume decreases, which is usually associated with decreased entropy. How is this resolved? In this case, the solvent becomes less ordered, but the polymer network becomes more ordered.

$$Q = m_s \int_{T_H}^{T_L} c_s(T) dt + m_n \int_{T_H}^{T_L} c_n(T) dt < 0$$

From point 3 to 4, the gel is isochorically cooled. The flow of heat is:

The negative sign indicates heat flow to the reservoir. From point 4 to 1, the gel expands isothermally. The heat transfer in this step is the combination of the latent heat in the state transition and the heat of the volume change:

$$\boldsymbol{Q_{ITE} = Q_{CL} + Q_{CW}}$$

Where Q_{CL} is the latent heat of changing state and Q_{CW} is the energy converted to work through

$$W = \int_{V_1}^{V_2} \pi(V) dV$$

volume change. The work done in this portion of the cycle is:

With this complete description of the gel cycle, the thermodynamic efficiency can be restated in a more general fashion. Therefore, this may be applied whether the gel is simply opening a one-shot microvalve, or is performing a more complex pumping function on the same chip. In the proposed application, the environment provides a heat sink, and the efficiency will be:

$$\eta = \frac{W_{23} + W_{14}}{Q_{12} + Q_{34}}$$

Chapter 5

HYDROGEL VALVES

Having developed a mechanically useful NIPA-based hydrogel and a model of its dynamics, a method must be developed to integrate the gel into the microfluidic network. Hydrogels are soft materials, and not well suited to surviving common processes used in micromachining. A few attempts were made at patterning the hydrogel inside a microchannel without photopatterning:

A. Micromolding: mold gel on substrate and then bond glass to the top of the channel. This method was unsuccessful since the high temp burnt the gel and rendered it useless.
B. Microextrusion: DRIE was used to etch holes from the backside of the wafer to the desired location of gel valves. The principle here was to drive hydrogel from the backside through the holes to form small cylindrical gels. This method was also unsuccessful. There was a significant pressure drop from the driving pressure required to push the gel through the DRIE holes and the pressure needed to push the gel through the microfluidic circuit. Thus, the gel would emerge from the DRIE holes and flood the entire network.

Therefore, lithographic techniques were developed to pattern the hydrogel. These too proved to be complex.

5.1 NIPA patterning by photocrosslinking

Kuckling et al[24] demonstrated a photocrosslinked NIPA hydrogel that may be patterned to features 20 μm in width. A photocrosslinked gel is more desirable than a photoinitiated gel since it offers a higher degree of resolution. Many chemical process steps are required to create the chromophore and bind it to the NIPA copolymer. The key reaction is a [2+2] cycloaddition of stilbazolium salts when exposed to UV light. This cycloaddition is thermally irreversible, yielding a new permanent crosslink. The stilbazolium salts consist of two structural parts, a hydrophobic stilbene backbone, which is necessary for crosslinking, and a pyridinium group, used to increase the phase change temperature. The effect of the pyridinium group offsets the decrease in phase change temperature introduced by the presence of the hydrophobic stilbene. The resulting polymer has the characteristics required, namely, a patternable NIPA hydrogel suitable for mechanical work. The results of this patterning are shown in Figure 19

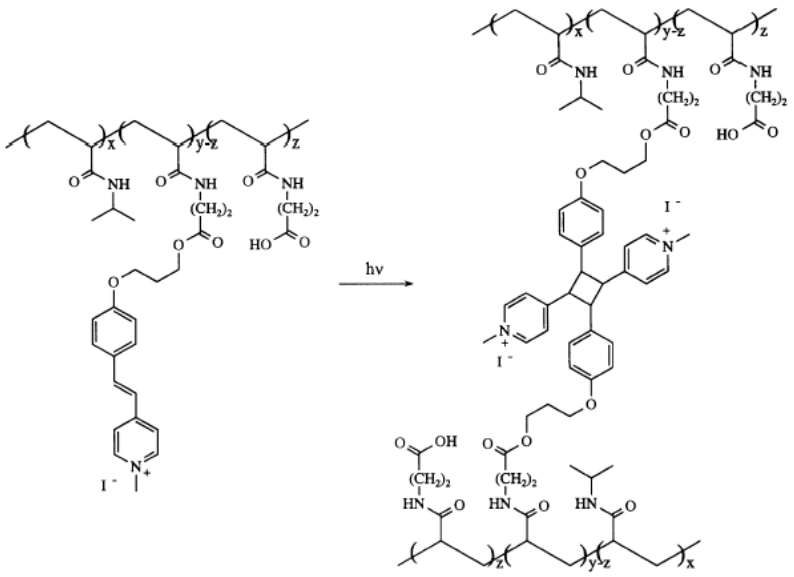

Figure 19: photocrosslinked NIPA hydrogel formulated by Kuckling et al.

The prepolymer was formed from a radical copolymerization of NIPA and 3-acrylamidopropanoic acid in dioxane with 2,2'-azobis-(isobutyronitrile), referred to commonly as AIBN, as an initiator. The photopolymer was formed from a synthesis of the prepolymer, 1-methyl-4-(2-(4-(3-hydroxypropoxy)phenyl)vinyl) pyridinium iodide, dimethylaminopyridine (DMAP), and dicyclohexyl-carbodiimide. The solution was acidified with hydrochloric acid. The precipitate was precipitated with THF/diethylether. Multiple attempts were made to repeat this formulation. Our efforts to re-create this chemistry were unsuccessful.

Still, this formulation of a photocrosslinkable MIPA gel may be considered the "gold standard" by which our results may be judged. The thermosensitivity of the photoreactive polymer is strongly weighted by the relative hydrophobicity of the chromophore. Other chromophores had been used by Kuckling et al[24], such as coumarin or cinnamate, but proved to be very hydrophobic. The stilbazolium salts used in the final formulation of gel were preferable because they carry a permanent charge, conferring hydrophilicity and a lower phase transition temperature.

The photocrosslinking was done on a dry film of polymer. Illumination was provided by a 400W UV lamp for wavelengths greater than 315 nm. For gel formulations with higher concentrations of chromophore, the irradiated polymers became insoluble in water. For chromophore concentrations less than 0.2% wt, a true network was not formed, and gelation was inhibited.

5.2 NIPA patterning via copolymerization and alternate photocrosslinking

Other gel chemistries were investigated. A copolymer of NIPA and acrylic acid (AA), terminated by mercaptoproprionic acid (MPA) was synthesized to allow other dyes to be bound to the gel. Nineteen parts NIPA were used for every part of acrylic acid. In particular, a photocrosslinkerr, 4-azidoaniline, may be bound to the copolymer of NIPA, AA, and MPA, as shown in Figure 20. Incorporation of the photocrosslinker should allow polymerization to be initiated by a low power light source. Therefore, the gel can be patterned via lithography. A subsequent wash will remove unreacted monomers. In published research this gel has been shown to retain its temperature sensitive response[25,26]. This should theoretically allow valve patterning to be done in situ on MEMS chip. Both the transition temperature and swelling ratio of the gel are reduced in comparison to regular NIPA gel due to these modifications. Although a reduced transition temperature is beneficial since less heat energy will be required, the reduced swelling ratio is not.

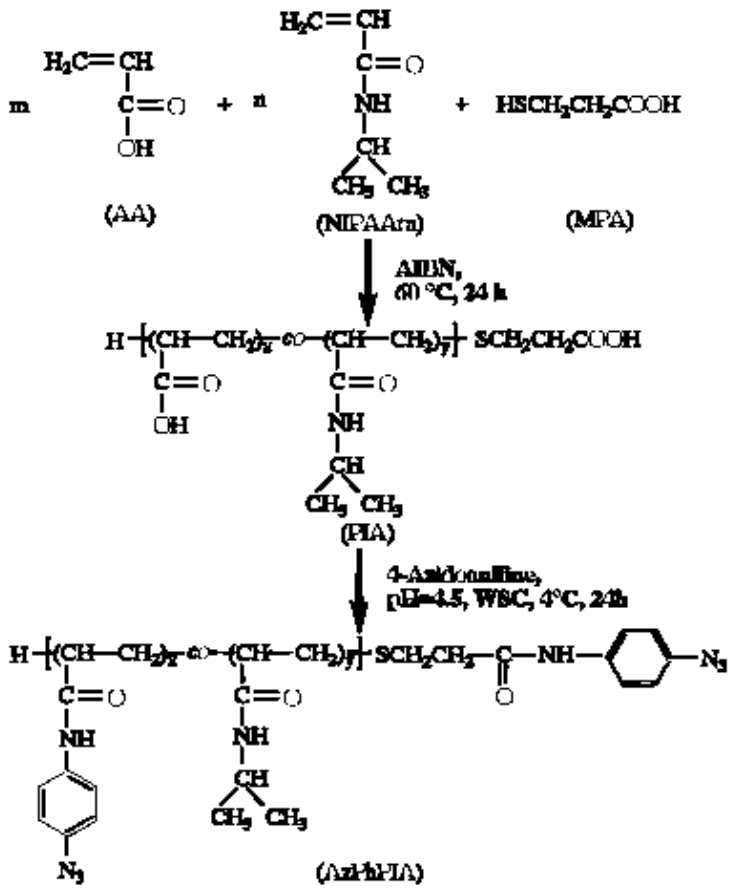

Figure 20: Synthesis of a lithographic NIPA hydrogel from Chen, Imanishi, and Ito

The synthesis was conducted per the references in Langmuir and Macromolecules. Unfortunately, the resulting gel was extremely fragile, and was invariably damaged in the process of patterning. Thus, the gel would hardly be suitable for mechanical work. However, the photoinitiator used, azobis-isobutyronitrile, may have another important application in pumping, described in chapter 6.

5.3 Liftoff technique of NIPA patterning

Since the published chemistries for patterning NIPA gel failed, we were forced to develop alternate means of patterning. We attempted to modify techniques commonly used in micromachining for patterning gel. A prerequisite for such a technique is a method to preferentially bind NIPA to silicon. Fortunately, researchers have demonstrated that vinyltrimethoxysilane (VTMS) is an excellent molecule for linking silicon to $NIPA_{27}$. According to Liang, VTMS may be introduced in a 5% (v/v) solution of toluene and heated to 100^0C to bind the molecule to silicon. A standard thick photoresist was patterned on silicon and VTMS was applied to create a pattern to bind NIPA. However, the VTMS was present everywhere on the wafer! Therefore, the toluene made it possible to for the VTMS to pass through the photoresist barrier. The experiment was repeated, using non-polar hexane instead of toluene and the silicon was successfully patterned with a monolayer of VTMS. This is shown pictorially in Figure 21:

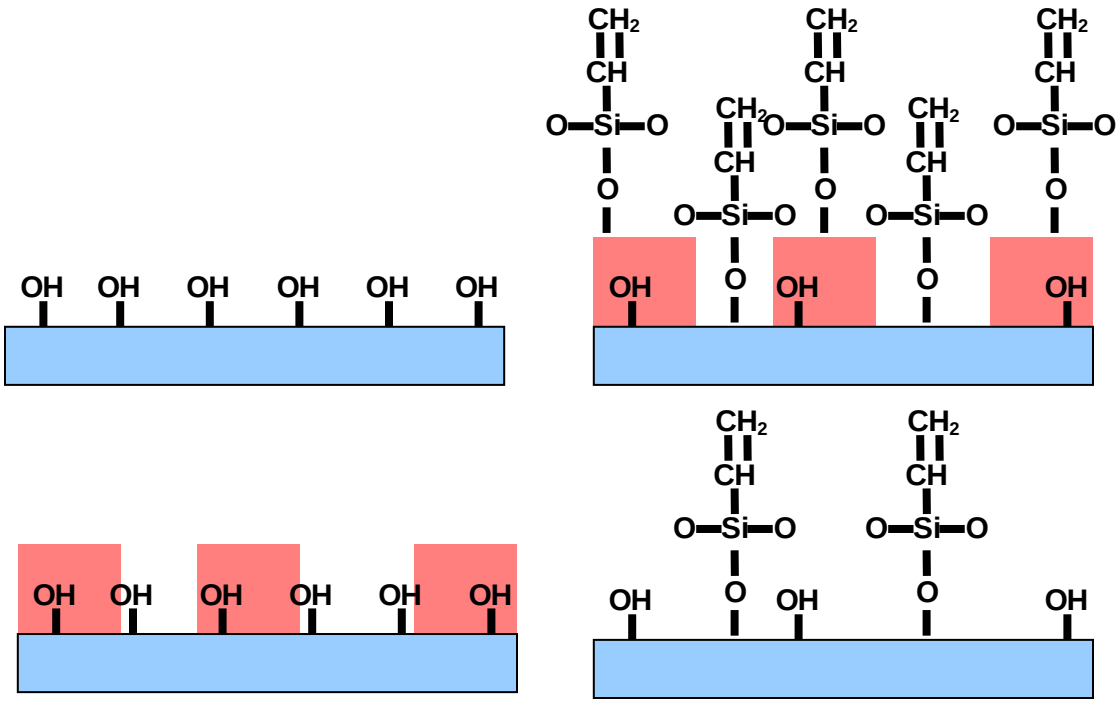

Figure 21: Method for patterning VTMS on silicon a) oxidize silicon, b) pattern resist on SiO2, c) introduce hexane/VTMS solution and heat to 100^0C, d) strip resist

With the VTMS patterned on the silicon, it appeared simple to use this pattern as a template to grow NIPA. NIPA gel could be initiated everywhere and then subsequently washed. The unbound gel would wash away, leaving patterned gel. This is illustrated in Figure 22.

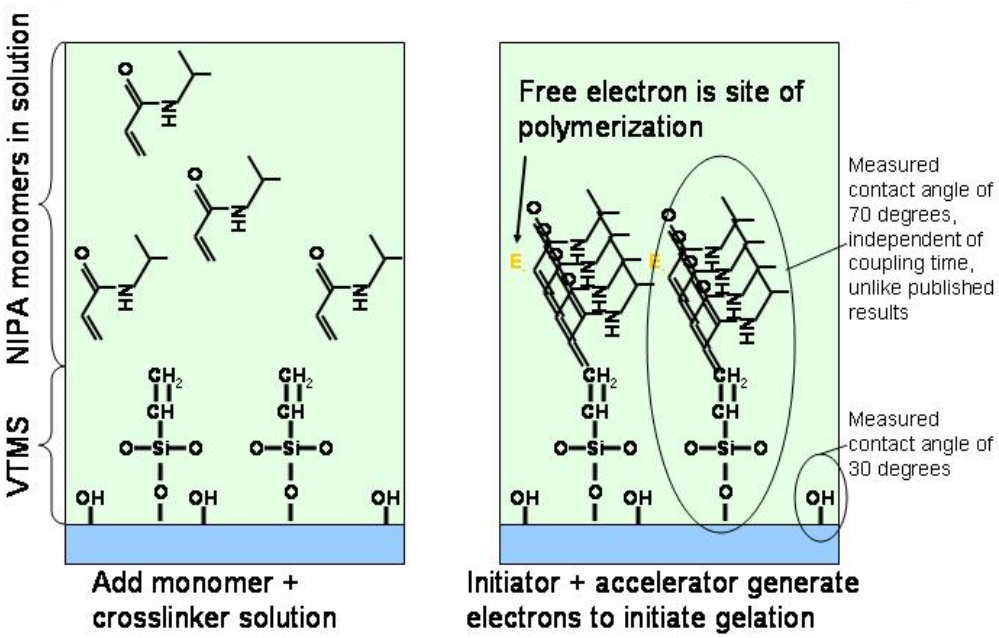

Figure 22: Proposed method to pattern NIPA gel via selective patterning of VTMS

Again, experimentation proved contrary to the proposed technique. The VTMS-coated areas of silicon are highly hydrophobic in comparison to bare silicon or silicon dioxide. The measured contact angle for the SiO_2 regions was 30^0, but the contact angle in regions of VTMS was 70^0. Therefore, the solution of NIPA monomers, crosslinkers, and initiators in water would bead up in regions without VTMS. In other words, the gel would form only in regions where it would not bind to the silicon. Silicon dioxide degrades over time, and becomes less hydrophobic usually within two days of deposition. The increase of hydrophobicity was not sufficient to overcome this problem.

5.4 Patterning NIPA gels via photoinitiation

Having failed to develop a suitable microfabrication technique or photocrosslinking method to pattern the gel, other alternatives were considered. Photoinitiation would be another suitable method to pattern gel, although the resolution of this technique may be inherently less than photocrosslinking. A photocrosslinker defines the volume where crosslinking takes place, and therefore defines the volume of the gel. A photoinitiation technique only defines the volume where initiation takes place, and therefore gelation can continue outside this volume.

After trial and error with commonly used photoinitiators, we found riboflavin to be useful when combined with TEMED and ammonium persulphate as accelerators. Under illumination, riboflavin decomposes to leucoflavin. No free radicals are formed without oxygen but small amounts of oxygen allow the leucoflavin to reoxidize with free radical generation. The free radicals initiate the gelation reaction. This is a key point, since other initiators must be used in a nitrogen environment. The use of riboflavin allows for simple in situ photopatterning in a benchtop setting. Using this technique, polymeric gels were synthesized by N-isopropylacrylamide (main constituent) and N,N'-Methylene-bisacrylamide (crosslinker), as shown in Scheme 1.

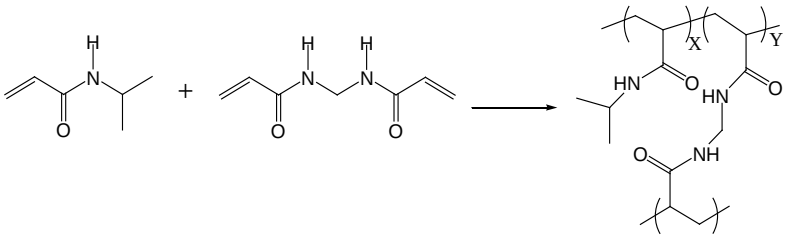

Scheme 1: NIPA gel formation using riboflavin as photoinitiator

The pregel solution consisted of 3.87g of NIPA, 0.348g Bisacrylamide, 105 μL of TEMED accelerator, 0.1 mg of ammonium persulphate, and 0.333mg of riboflavin in 50 mL of deionized, purified water at room temperature. This formula was based on similar recipes for generic gels used for DNA separation and experimental results identifying robust gels. Simple transparency masks were used to test the different pregel formulations. The pregel solution required a couple of minutes' exposure from an 8.0mW/cm^2 Fisher Scientific Transilluminator source. This uncollimated light source only allowed very rough patterning.

Since this was an entirely new technique for patterning, we developed a quantitative method to verify that gelation had occurred. Fourier Transform-Infrared (FTIR) was used to confirm gelation had successfully occurred with this new technique. Figure 23 is the FT-IR results from the gel. There is noise on the signal due to the presence of water, but the most important point in this figure is the peak at wavenumber 3300. This particular wavelength corresponds to N-H bonds that can only be present for successfully gelated NIPA.

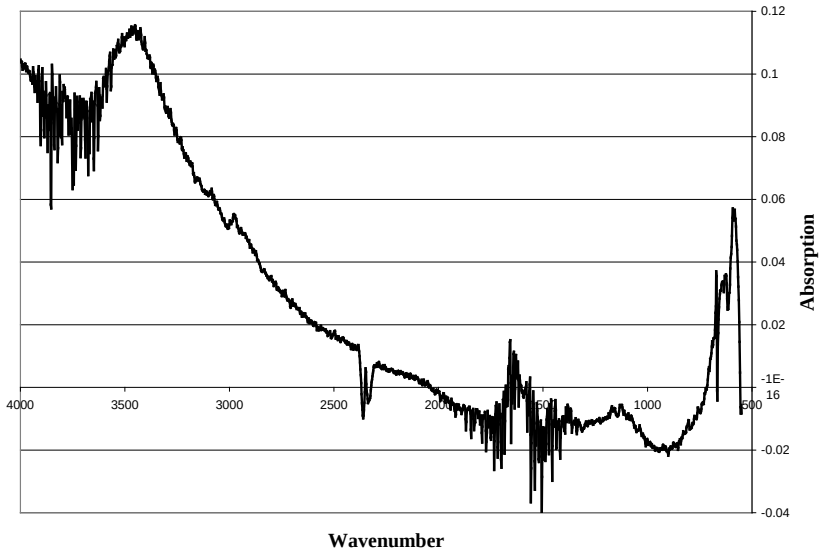

Figure 23: FT-IR Absorption of NIPA hydrogel photoinitiated with riboflavin

Using this patterning technique our group has patterned cylindrical and cubic gel structures down to 50 μm in width. Environmental SEM pictures were taken of several mm diameter gel patterned on a flat surface shown in Figure 24. These gels were photoinitiated through a perfectly circular pattern on a transparency mask. Therefore, without a sidewall to contain the prepolymer solution, the gel forms an arbitrary shape. These pictures illustrate the uniformity of the gel in the z-dimension, and the structural integrity of the gel when created with this method.

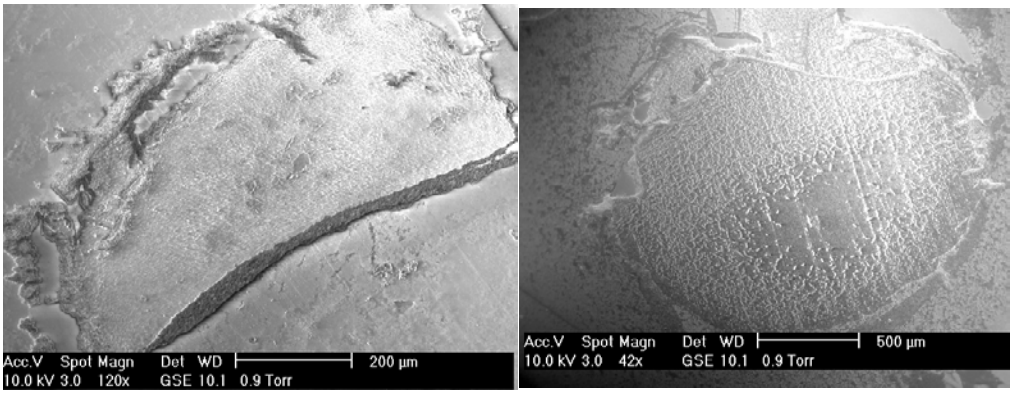

Figure 24: Environmental SEM of NIPA gel patterned with new technique

5.5 Microvalve Fabrication

Once the hydrogel was developed, characterized, modeled, and successfully patterned in situ, the gel could be utilized in microscale applications. Experimentally, the gel requires at least a 20μm diameter circular pattern to initiate a structural gel. For any features larger than that, the gel structure is only limited in the x and y dimension by the pattern of the mask.

Standard silicon micromachining techniques were used to create simple chambers and channel in silicon shown in Figure 25. The microvalves and channels were patterned lithographically on silicon wafers on the front of the wafer with AZ5214 resist and AZ4620 resist on the backside. The silicon was then machined via deep reactive ion etch (DRIE). The topside of the wafer was patterned with the microfluidic test structures. The main flow channels were 200 μm in width, and the valve structures varied from 50 μm to 500 μm. Holes were etched from the bottom of the wafer through to the top, allowing fluidic connects to be glued to the bottom. Pyrex glass was anodically bonded to the silicon at 400^0C and 1000 V, resulting in complete channels.

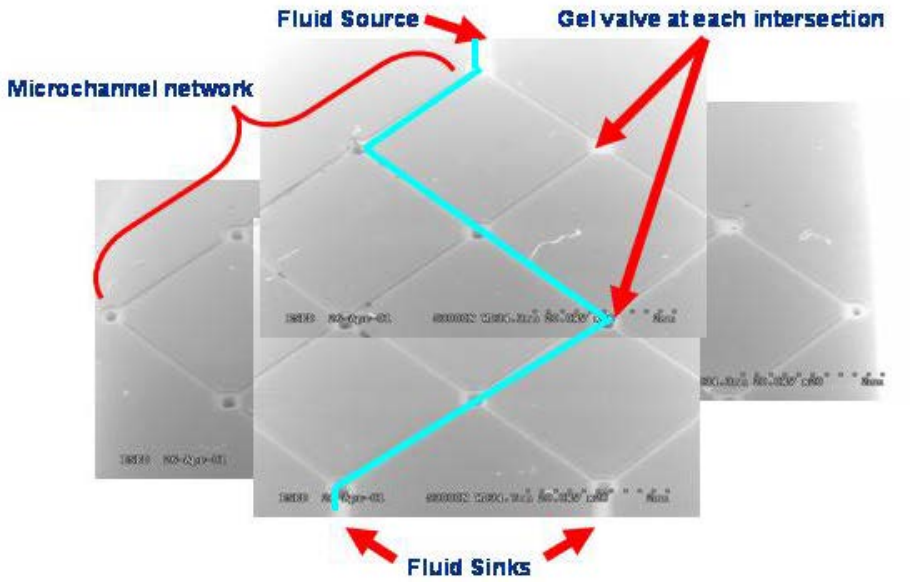

Figure 25. Silicon micromachining produces 2D network of channels and nodes for gel valves

The pregel solution was injected into the microchannels. Another mask was used to lithographically pattern the gel through the pyrex cover into circular and square shapes. The solution required 20 minutes of 8.0 mW/cm^2 exposure to gelate. Collimated light from a Karl suss aligner allows for gel structures with higher definition. The substrate was then heated to collapse the valving structures and release the unused pregel solution as shown in Figure 26. Room temperature deionized water seeded with 4μm diameter fluorescent beads was used to characterize the opening and closing of the valves.

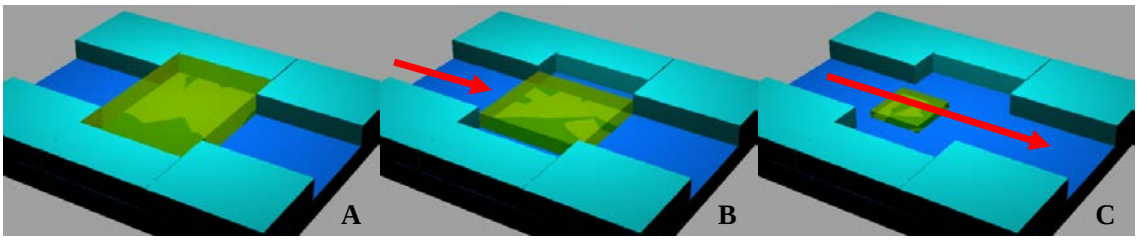

Figure 26. Conceptual schematic of heat activated microvalve. Hydrogel structures are patterned in situ using lithography (A). Heating the gel induces the gel to shrink (B) and open the valve (C).

5.6 Microvalve Testing

The valving function of the gels was tested. The substrate was heated to 33^0C to induce gel collapse, which is shown in the first row of Figure 26. When external heating is removed the gel swells and closes the valve, as also shown in the second row of Figure 27.

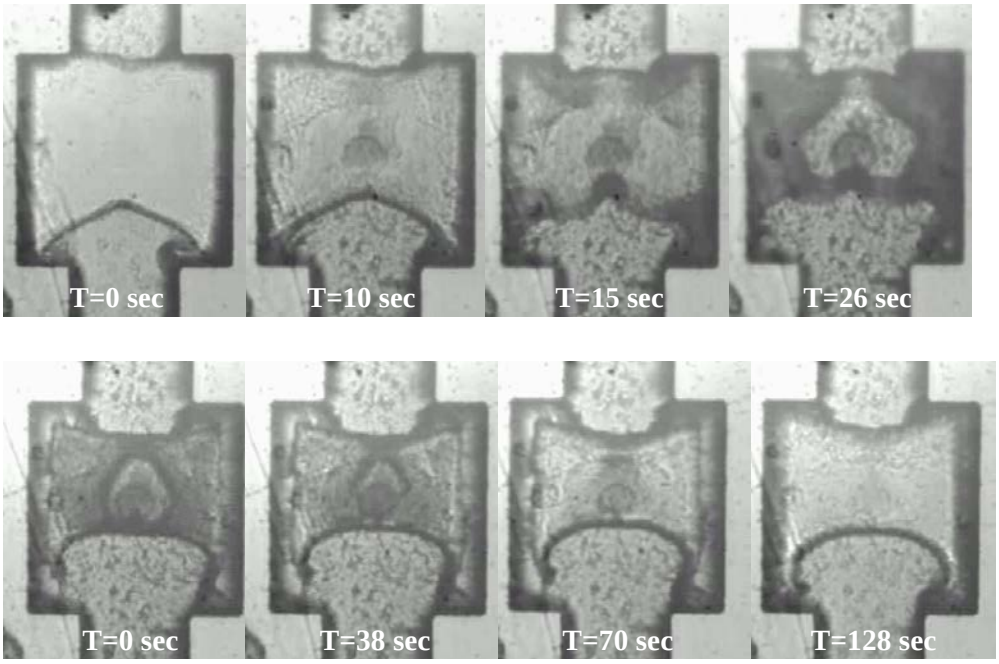

Figure 27. Collapse and expansion of a 200 um x 200 um x 75 um hydrogel valve. Series A shows the opening of a valve as heat is applied. Series B depicts the closing of the valve as the gel swells via diffusion

Gel collapse and release of most of its water occurs in less than thirty seconds. Once the gel returns to room temperature, the gel becomes hydrophilic and regains its shape via diffusion after two minutes. These results are in close agreement with experiments of free floating NIPA gel spheres 200μm in diameter described in Section 3.2. The time constant is an order of magnitude different between these two motions, due to the differences between the collapse mechanism and expansion mechanism.

The full range of gel valve motion was measured with a visual basic program. Then, individual points on the outer radius of the gel were measured with respect to time to determine the time history of the valve opening and closing. This is plotted in figure 27.

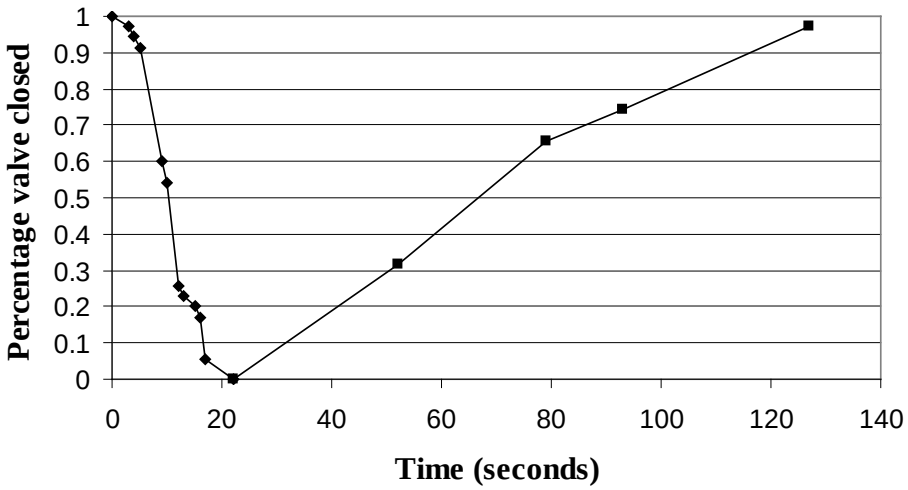

Figure 28. Gel valve opening and closing via water release and absorption versus time

Chapter 6

GAS EMITTING PUMPS

6.1 Prior AIBN pumps

In section 5.1, a gel was fabricated using azobis-isobutyronitrile (AIBN) as a photoinitiator. In a recent article, Ahn used AIBN to generate nitrogen gas within a microreaction chamber as a pump[28]. The schematic for this micropump is shown in Figure 29.

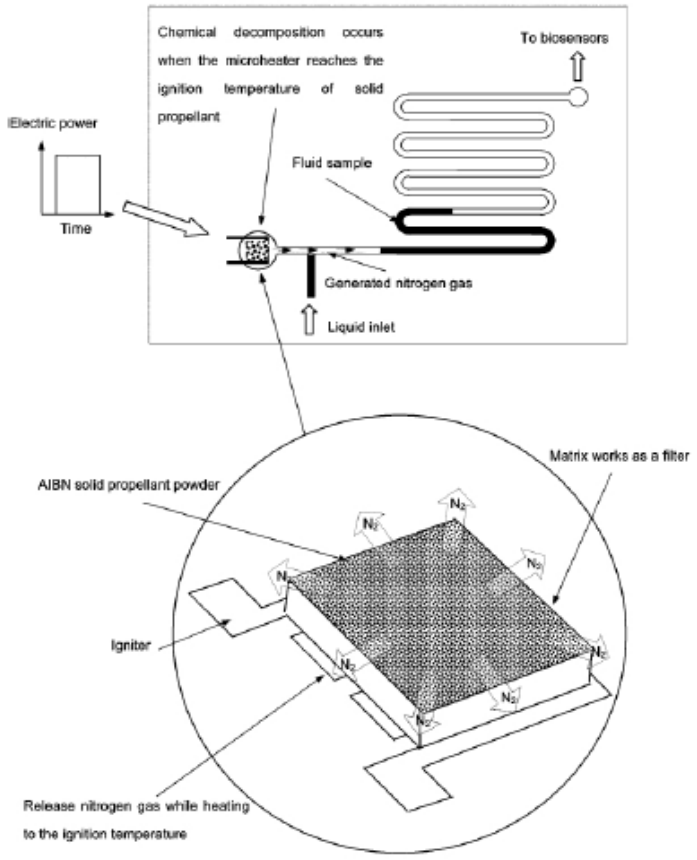

Figure 29: Schematic of AIBN-based micropump developed by Ahn[28]

AIBN offers several advantages as a high-pressure actuator. Liquid propellants require more sophisticated holding and metering systems to control their release. Conventional solid propellants may be a good choice for microsatellities, but they produce toxic gases, and often require temperatures above 400^0C to produce an optimal reaction. Significantly, the AIBN-based pump produced 3kPa of pressure when 187mJ of energy was applied to 100 μg of AIBN.

Ahn's group developed their pump by fabricating simple microheaters on a plastic substrate. They then patterned AIBN on the heater by using screen printing. The AIBN was mixed with Teflon to act as a matrix. Then, the Teflon/AIBN mixture was extruded through a steel stencil onto the heater. The package was then sealed and tested. The use of a steel stencil is a simple method to pattern such a material, and does not lend itself to mass production of inexpensive devices, nor carefully controlled pumps.

6.2 Novel AIBN pump design

To fabricate novel micropumps, we have incorporated significant quantities of AIBN into patterned PDMS wells. Patterned PDMS wells permit multiple pumps to be incorporated into a single unit, and allow for superior control of propellant deposition. When the microfluidic circuit is joined with microheaters, it is possible to heat AIBN to the temperature necessary for decomposition and release of N_2. This technique allows in situ fabrication of pumps in addition to valves, fulfilling the original goal of an integrated system of valves and pumps for lab-on-a-chip.

To achieve the desired complete circuit, AIBN pump design consists of the following four design elements:

1. Determine the number and magnitude of fluid perturbations necessary to induce chaotic mixing. Design sufficient number of single-use pumps to provide serial pulsing of fluid flow.
2. Determine method to isolate fluid flow from gas emission as pump fires.
3. Design microheater to provide necessary heat for firing.
4. Build system and characterize performance.

These will be reviewed in turn.

Chaotic mixing in microchannels will be more fully explored in the next chapter. For pressure-driven mixing induced by folding, two perturbations are required to create a single fold. Multiple folding events are required to establish consistent mixing. Numerical investigations revealed that the first 1-3 periods are used to establish the flow pattern, and at five periods a consistent flow field is established. The magnitude of the pressure must be sufficient to overcome the backpressure of the system, and cause the alternating flow to pass the saddle point. For our mixer design, we will assume that a vacuum of equal magnitude to the positive pressure of the pump may be used in alternation. Based on Hagen-Poiseuille flow, the pressure necessary to drive a sucrose solution at 20cP through a 100um width by 200um depth channel at 500um/sec is 0.125mPa. Therefore, we will need at least five pumps on either side of the mixing section, and each must deliver 0.125mPa to fulfill design element 1.

For design elements 2, the pump, we must advance the AIBN technology in several ways. An encapsulated lab-on-a-chip must allow multiple fluid processing steps, typically culminating in a detection event. Sensing technologies must be carefully calibrated to the analyte, and uncontrolled multiphase mixtures are incompatible with these technologies. Thus, the driving gas must remain separated from the fluid. Prior work has isolated working fluid in a microfluidic delivery system via a drop of oil. However, for our work, both positive pressure and vacuum are required. Thus, we choose to isolate the AIBN/N2 via a thin layer of PDMS.

Rather than pattern the AIBN via a stencil, we use PDMS to define AIBN deposition. Multiple heaters are patterned and fabricated via surface micromachining techniques.

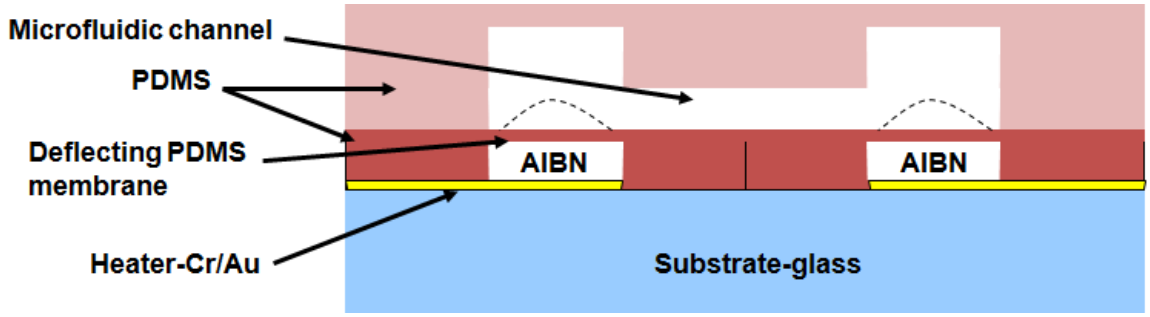

Figure 30: Design of AIBN-based micropump

For the design in figure 30 to be successful, the PDMS must have sufficient deflection and elasticity to pump the requisite volume of fluid. The volume of fluid in the mixing region is only 2 picoliters, so the volume is set to accommodate deformation and leakage of the system. In our system, we have designed the AIBN pumps to deliver up to 700pl of fluid.

Proceeding to a design that may be manufactured, we require two different heights to achieve a multi-pump design that may be incorporated into a micromixer:

1. Height required for mixing channel~100 μm

2. Height required for individual pump element~1 mm

These are illustrated in the figure 6 previously. The “fluid source”, “fluid sink”, “pump sources”, and “gas-emission pump” elements are all designed for the 1-mm thickness. To achieve this, two SU8 fabrication processes were developed. SU8-2025 was used to develop a consistent 130+/-10μm thick process. SU8-2100 was used to develop a 260+/-20μm process. These processes were used in series to create a 4 layer multistack. The first layer was used at ~130um to define fluid channels, and the next three layers were used to create the large fluid sources et al. The resultant mold is shown in figure 31:

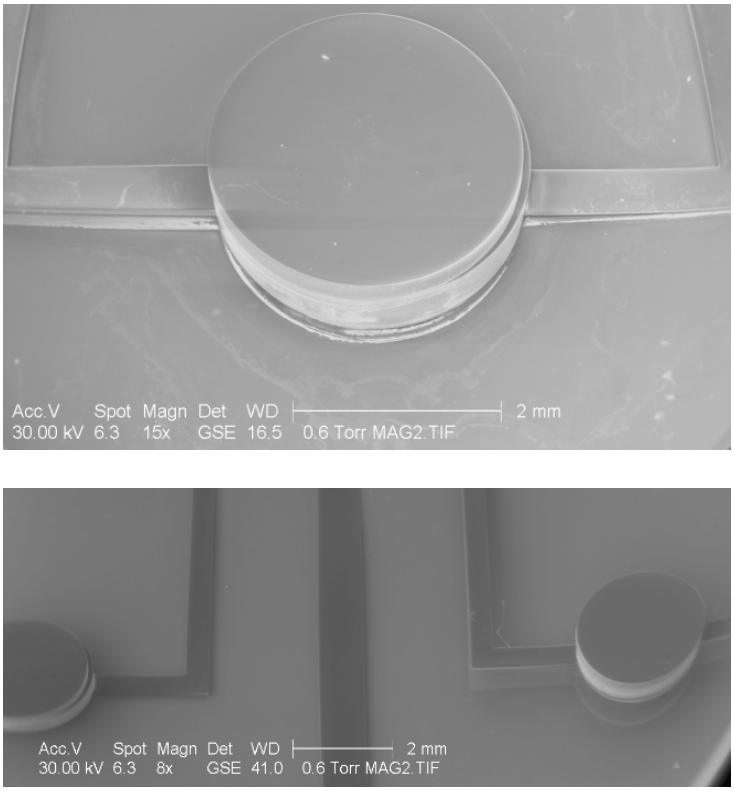

Figure 31: completed SU8 mold

Layer registration was limited by the accuracy of the fiducials that were developed for each layer, and was typically on the order of <20μm. A separate mold was used to define the

individual AIBN wells, based on the same process flow. In addition to the SU8 master molds, the PDMS films required a mating surface to create a repeatable thickness. This was most critical to define the PDMS layer between the AIBN emission and the working fluid layer, which was targeted to be 100um thick. Consistent variation was found from mold to mold operation on the order of 10μm.

6.3 Heater design and test

For design element 3, a simple set of chrome and gold electrodes to drive AIBN decomposition were designed and fabricated. 200 angstroms of chrome and 800nm of gold were deposited by e-beam evaporation and patterned lithographically. To design the pattern of the electrode, multiphysics analysis was conducted was conducted with a commercial multiphysics finite-element analysis software suite known as COMSOL. Multiphysics analysis is used since thermally resistive heaters are described by coupled physics equations. As the metal conducts electricity, Joule heating increases the temperature. The heat, in turn, has an impact to the conductivity of the metal. This couples the physics. The electronic current balance is defined by the equation

$$\nabla \cdot (-\sigma_{metal} \nabla V) = 0$$

where σ_{metal} denotes the electrical conductivity of the chrome and gold. The conductivity is a temperature dependent function given by the expression

$$\sigma_{metal} = \frac{1}{\rho_0(1 + \alpha(T - T_0))}$$

where ρ_0 is the reference resistivity at a reference temperature and α is a proportionality constant. The thermal balance equation is given by:

$$\nabla \cdot (-k_T \nabla T) = Q_{\text{electric}}$$

where the heat source is

$$Q_{\text{electric}} = \sigma_{\text{metal}} |\nabla V|^2$$

k_T is the thermal conductivity of chrome and gold. A steady state analysis was used to predict the temperature profile of the heater and PDMS cavity to ensure the entire cavity would reach the target temperature of 95^0C.

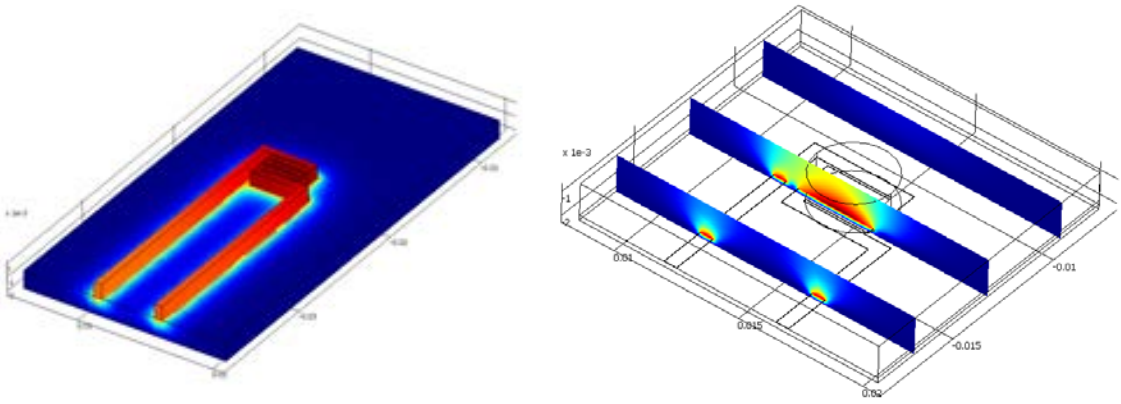

Figure 32: temperature profile for AIBN wells.

In Figure 32, red denotes temperatures >100^0C and blue represents room temperature. To validate this design, and investigate dynamic behavior, the heaters were tested at a variety of voltages across time. Figure 33 illustrates the test setup, and figure 34 depicts the thermal response of the heaters versus time.

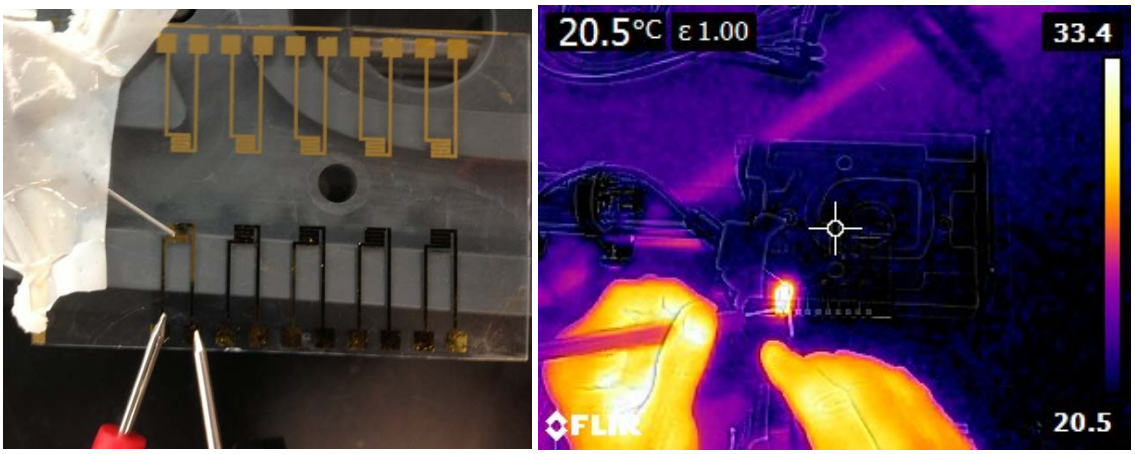

Figure 33: fabricated heaters and thermal imaging of heater

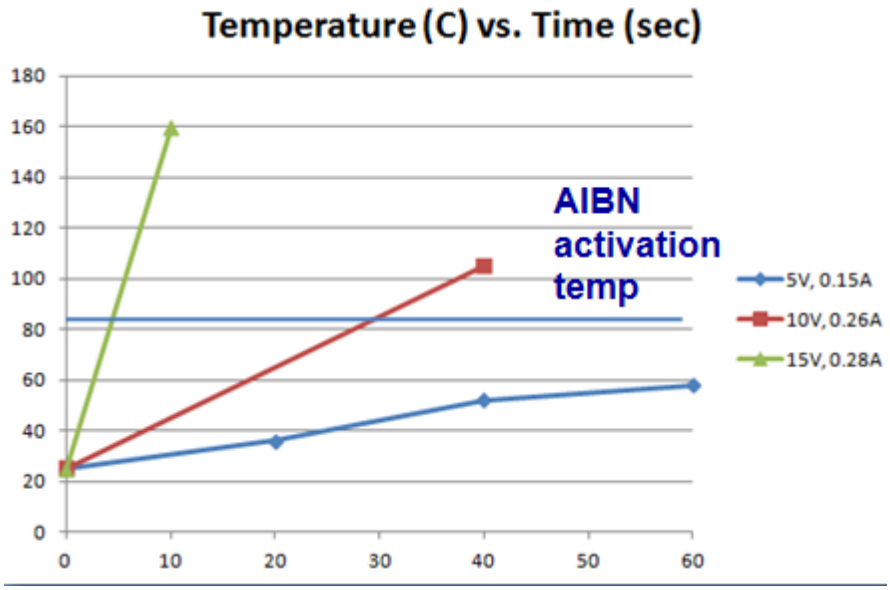

Figure 34: temperature vs. time as a function of driving voltage

Thus, to achieve the required temperature profile in less than 5 seconds, at least 15V of driving voltage is required. Since the range of periods for mixing is in the range of 2.5-7.5 seconds, the time delay for the heaters to achieve the required temperature must be considered when designing the firing sequence.

6.4 Membrane design and fluid-structure analysis

For the fourth design element, fabrication of the pump and characterization, additional multiphysics analysis was conducted to determine the requisite thickness of the PDMS deflection layer and the time constant of the pump response.

In this multiphysics simulation, the outputs are the time to maximum deflection of the PDMS membrane, and an assessment of whether the range of membrane thicknesses that could be consistently fabricated with our process was suitable for our pump design. As the AIBN emits nitrogen, pressure increases in the well, which causes the PDMS to defect. In the final design, each well is isolated, and the ideal gas law

$$PV=nRT$$

may be used to calculate the pressure in the well. In the original design, the wells were all connected by a common fluid path. The wells were fired locally to displace each pump locally. In this case, there is both a low-Reynolds number fluid dynamics problem to solve, and a large-deflection structural mechanics problem for the PDMS. This is a challenging problem, since the deflection of the PDMS results in a change to the flow field.

To solve this problem set, we use the arbitrary Lagrangian-Eulerian (ALE) technique for a continuously deforming geometry. The ALE algorithm addresses the dynamics of the deforming geometry and the moving boundaries with a grid that moves. COMSOL computes a new mesh based on the motion of the PDMS membrane at each time step. The Stokes flow expression of the Navier-Stokes equations are computed for each time step. The problem was solved for a 2-D

flow. Since the 3-D geometry is more difficult to displace, a radius-dependent correction factor was added to a Mooney-Rivlin model for the modulus of PDMS. The Mooney-Rivlin relationship is an empirically derived strain energy density function. The problem was defined with the geometry outlined in figure 35:

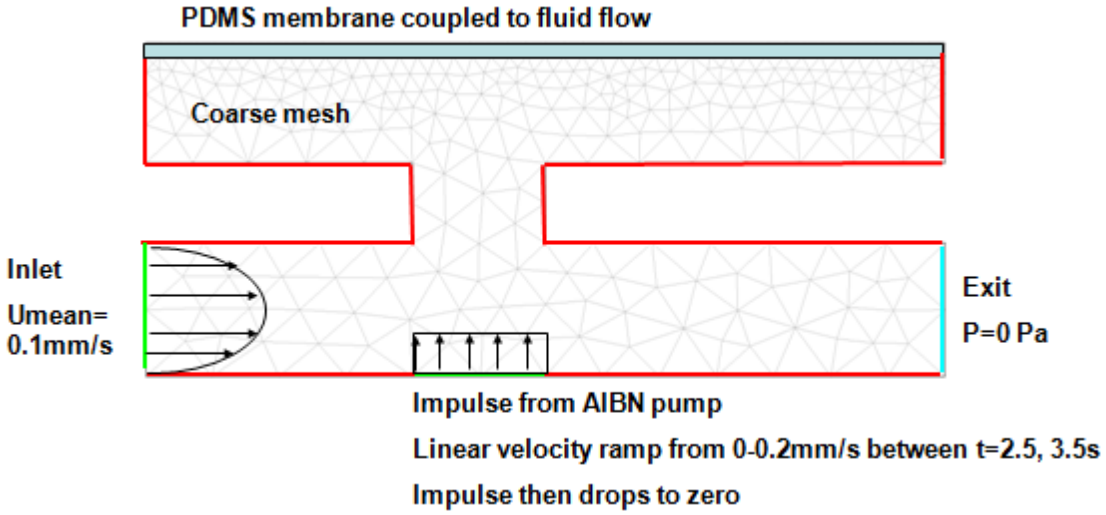

Figure 35. Analysis conditions and applied finite-element mesh

The fluid flow in the system is described by the Navier-Stokes equations for the velocity field and the pressure in the deformed moving coordinate system.

$$\rho\frac{\partial \mathbf{u}}{\partial t} - \nabla \cdot [-p\mathbf{I} + \eta(\nabla \mathbf{u} + (\nabla \mathbf{u})^T)] + \rho((\mathbf{u} - \mathbf{u}_m) \cdot \nabla)\mathbf{u} = \mathbf{F}$$

$$-\nabla \cdot \mathbf{u} = 0$$

The PDMS boundary condition experiences a load from the fluid which is the sum of pressure and viscous forces.

$$\mathbf{F}_T = -\mathbf{n} \cdot (-p\mathbf{I} + \eta(\nabla \mathbf{u} + (\nabla \mathbf{u})^T))$$

The time step approach to fluid flow solution also enabled a large-deflection solution for the structural mechanics problem. The motion of the deformed mesh is modeled using a technique

known as Winslow smoothing. The resultant deformation of the membrane is depicted in figure 36.

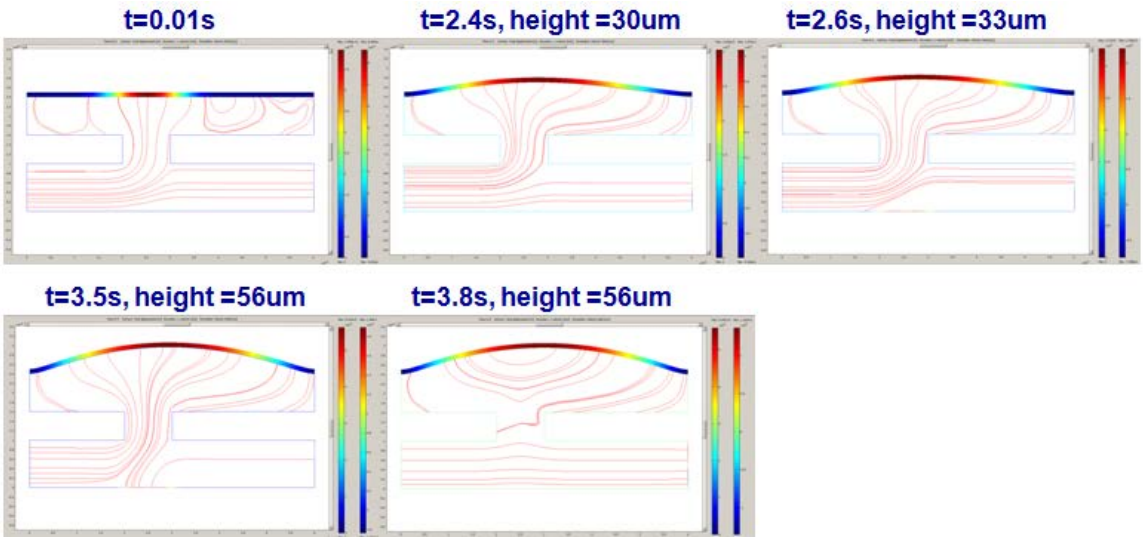

Figure 36: deformation of a PDMS membrane versus time.

These results illustrate that a connected series of AIBN actuators will achieve maximum deformation within 3.5 seconds. The total volume displaced per well is on the order of 100pl. However, the displacement is very sensitive to the thickness of the membrane, as well the parameters chosen for the Mooney-Rivlin model of the PDMS. For a single well, which was our final design, the response time is in less than a second.

6.5 Completed system and test

The integrated system is shown in figure 37, consisting of microheaters, AIBN-filled microwells, and thin-membrane/microfluidic actuation layers.

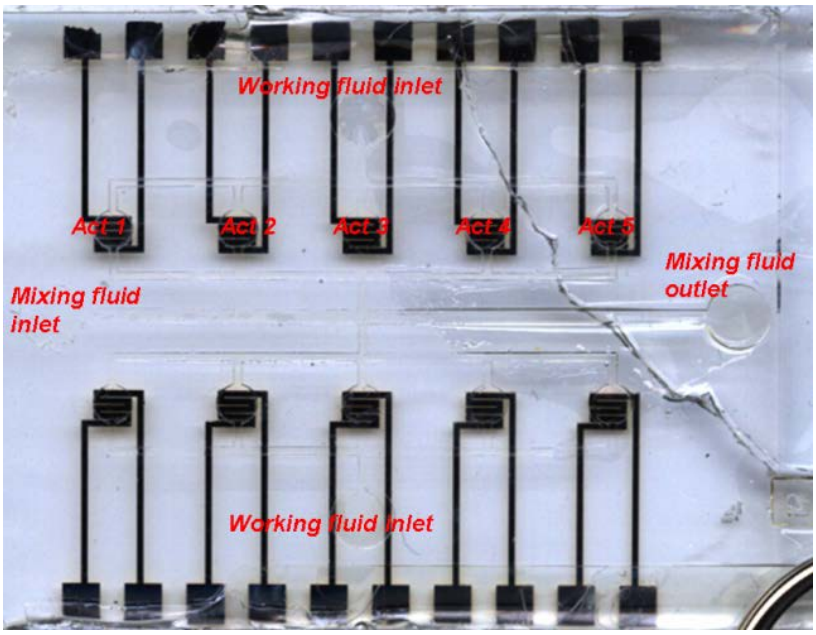

Figure 37: completed system

Each individual pump was tested for multiple wafers. Across all builds, high variability in pump deformation was demonstrated. This was due to the high variability in membrane thickness as described in section 6.4. In addition, the membranes were prone to burst, as shown in Figure 38:

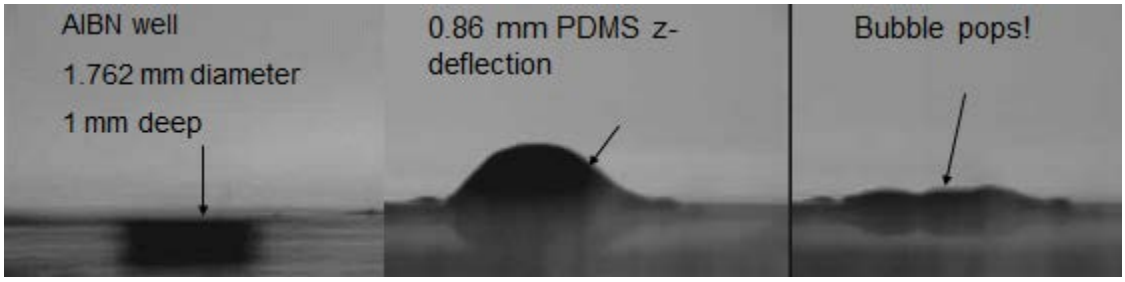

Figure 38: cross-sectional view of pump deformation

Chapter 7

OPTIMIZATION OF A MICROFLUIDIC MIXER

Now that pumps and valves have been demonstrated, they must be incorporated into a micromixer to complete the list of required lab-on-a-chip functions. To understand the micromixer opportunity in this research, a brief review of micromixer work done to date is conducted. Our intention is to design an optimized micromixer compatible with the AIBN pump we've developed.

7.1 Prior micromixers

Extensive micromixer designs, analyses, and testing have been conducted to reduce the time to mix two or more microfluidic solutions required by standard diffusion [29-31]. Both passive and active techniques have been developed. Active actuation techniques include pressure-based perturbation, acoustic waves, dielectrophoretic forces, electro-osmotic flows, thermal actuation, magneto-hydrodynamic forces, and magnetic beads. Passive techniques have relied on lamination, zigzag channels, barriers, twisted channels, or surface chemistry. The overall objective of these mixers is to achieve mixing of biological reagent solutions quickly, in a small space profile, with minimal power and complexity, via a technology that is easily transferable to manufacturing. Many of these mixers achieve the first set of goals. However, the transition to wide commercial presentations has remained elusive. The technologies developed in this thesis are attempts to ameliorate the manufacturing issues. However, these technologies have limitations of their own. The hydrogel valves are easy to manufacture and actuate, but are weak

and do not achieve sub-second performance. The AIBN pumps are powerful and simple, but require a time delay and are challenging to manufacture repeatedly with lab-based prototyping. The AIBN pumps fire once only, and are best used in a pressure-perturbation scheme. Multiple researchers have investigated a variety of pressure-perturbation schemes [32,33]. Notably, two perturbation schemes have been extensively studied, depicted in Fig 39.

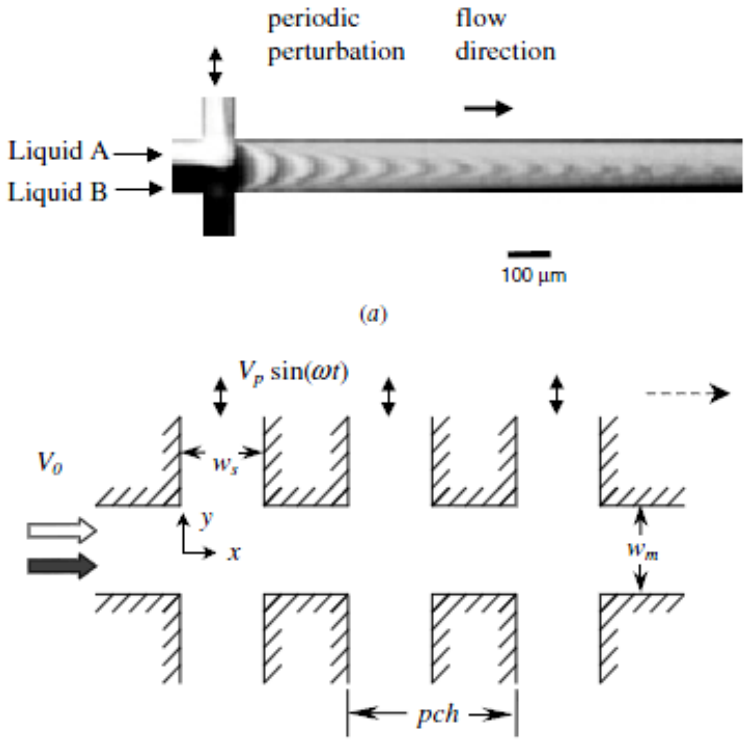

Figure 39: perturbation driven micromixers from Ref 33

In these studies, experimental studies were conducted to assess mixing, and numerical studies were conducted to determine pathlines and divergence. Before those results can be discussed, the methods of characterizing mixing must be understood.

7.2 Methods to characterize chaotic mixing and governing equations

Two fluids being mixed will evolve from separate and distinct homogenous bodies to a uniform and equal combination of the two given sufficient time and thermal energy. Diffusive mixing relies on thermal, or Brownian motion, to engage in molecular exchange across interfaces. Since diffusion occurs at time and length scales inappropriate for lab-on-a-chip applications, chaotic advection is necessary to complete mixing in a sufficiently efficient manner. Chaotic advection is characterized by growth of fluid filaments at an exponential rate, as shown in Figure 40. In other words, a small perturbation between two pathlines will rapidly diverge.

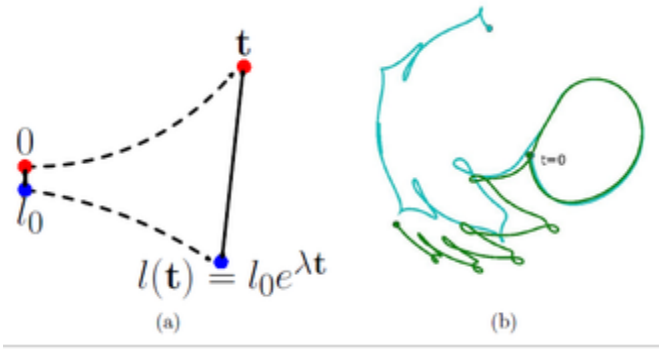

Figure 40 from Ref 34

A The exponential dependency on time is a key characteristic of chaotic advection

B Two pathlines for adjacent particles stirred by a rod moving in a figure eight motion

Sprott offers a clear and succinct definition of chaos as "the aperiodic, long-term behavior of a bounded, deterministic system that exhibits sensitive dependence on initial conditions"[35]. Chaos theory states that at least three degrees of freedom are necessary for a dynamic system to be chaotic. Three dimensional flows may result in chaotic advection, except when the flows have symmetries that reduce the degrees of freedom. For in-plane microfluidic flows, such as the

present case, a plane of symmetry exists in the midplane of the device, and there is insufficient freedom to invoke chaos. Other researchers have successfully built microfluidic circuits with out of plane components that satisfy this condition. As an alternative to a third spatial dimension, time may provide the necessary freedom of motion to induce chaos. In 2-D steady flow, the streamlines and pathlines are identical, and thus, limit the motion of particles. Time dependent 2-D flows may be used to produce chaotic advection.

In chaotic flow, particles that are initially separated by a small perturbation distance, will diverge trajectories exponentially. There are multiple methods to quantify this divergence: Lyapunov exponents or direct measurement of mixing.

A Lyapunov exponent is a mathematic expression to characterize the divergent behavior of a system. A finite time expression has been developed [32]

$$\lambda(\tau) = \lim_{|dX|\to 0}\left[\frac{1}{\tau}\ln\left(\frac{dx(\tau)}{dX}\right)\right]$$

Lyapunov exponents have two essential elements: the sign indicates chaos and the magnitude indicates the degree of chaos. They are always real numbers, and their magnitude represents the separation between pathlines in the case of fluid flows. The number of exponents is determined by the degrees of freedom of the system. The Lyapunov exponent is calculated from the flow field motion, and therefore only requires solution of the Navier-Stokes equations. This offers an advantage in minimizing computation time. The downside of this metric is that it may not be experimentally verified as an abstract concept.

An alternate choice for the figure of metric is to simulate both the fluid dynamics and convection-diffusion equations and calculate the change in concentration across the exit. This is not a trivial matter. Careful consideration must be given to the time and space discretization for both sets of equations. For incompressible flow, we use the following description of Navier-Stokes:

$$\rho\frac{\partial \mathbf{u}}{\partial t} - \nabla \cdot \eta(\nabla \mathbf{u} + (\nabla \mathbf{u})^T) + \rho \mathbf{u} \cdot \nabla \mathbf{u} + \nabla p = 0$$

$$\nabla \cdot \mathbf{u} = 0$$

Where η is the dynamic viscosity (kg/(m*s)), u is the velocity (m/s), ρ is the fluid density, and p is the pressure (Pa). The convection-diffusion equation is given by:

$$\frac{\partial c}{\partial t} + \nabla \cdot (-D\nabla c) = R - \mathbf{u} \cdot \nabla c$$

Where c is the concentration, D is the diffusion coefficient, R is the reaction rate, and u is the flow velocity. For our calculation, R=0 because no reactions take place. By solving both time-dependent equations in discrete time steps, the mixing of the system may be simulated. To define the mixing, we will use the same metric that experimentalists use, which is the root-mean-square deviation of the concentration for each point in the flow field:

$$I_E = 1 - \frac{1}{\overline{C}}\sqrt{\frac{\sum (C(x_2) - \overline{C})^2}{N}},$$

Where N is the number of pixels, x is the spatial dimension of interest, and the average concentration is given by:

$$\overline{C} = \sum C(x_2)/N.$$

For our simulation, values are calculated at the nodes of the mesh, and the concentration values are interpolated across the exit. Since we wish to calculate the net effect of mixing, instantaneous values are not relevant. We must conduct the simulation for a sufficient number of perturbation cycles to ensure consistent behavior over time. In addition, we calculate the mixing index across the exit and for a number of time steps equal to one full period. Although this approach is prone to artificial diffusion, there is a distinct advantage since the results may be verified against experimental results. For our work, we choose to use the mixing index as our figure of merit.

7.3 Problem definition

Our goal is to optimize our micromixer design to achieve the greatest mixing index. To optimize the design, we have many variables to choose from. Framing the problem properly informs the choices for optimization variables. We model the problem in such a way that prior experimental work may be used to validate our results. We will use a solution suitable for biological reagents. In this case, a sucrose solution with μ=20cP and ρ=1230 kg/m^3 at room temperature is used. Thus, for our model, the flow is modeled with incompressible Stokes flow since the Reynolds number

$$\mathrm{Re} = \frac{\rho \mathbf{v} D_H}{\mu} :$$

for our geometry, flow rate (u=1mm/s), and viscosity is Re=0.008. The low Reynolds number indicates that viscous forces dominate inertial forces. The two solutions to be mixed are a solution with and a solution without Rhodamine dye, with diffusivity D=3.1e-11 m^2/s. For

modeling purposes, the viscosity will not be dependent on variation in concentration, since this is a small effect. We will also apply our model to mixing of dilute solutions. Neither multiphase physics nor accretion will be considered. We define the geometry on a derivative of the previously fabricated multi-pump device:

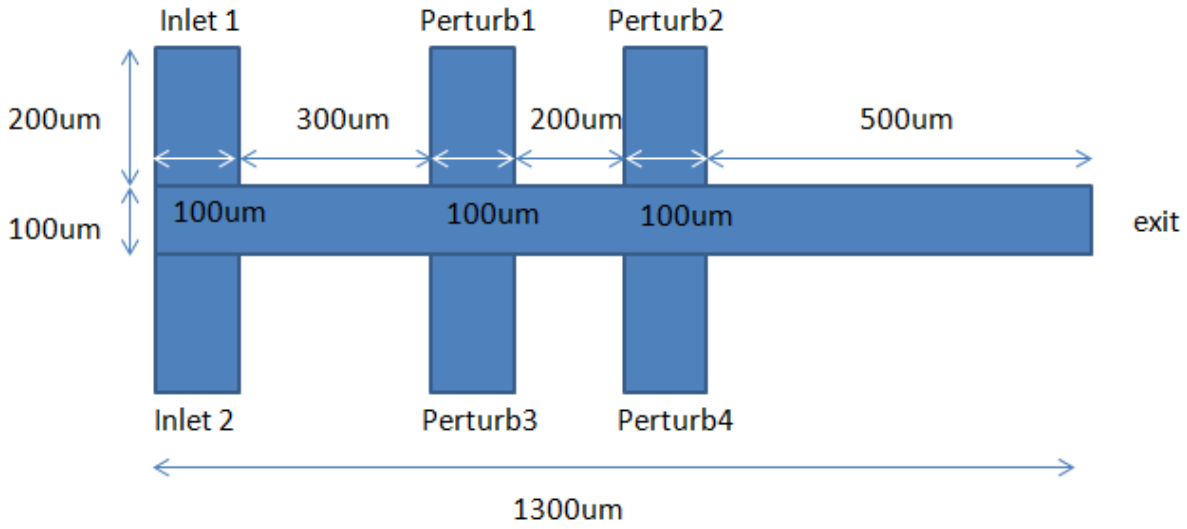

Figure 41 Model geometry

In our fabricated geometry, multiple pumps were used to create a cross-stream pulse at a single axial location. In this new geometry, we allow two cross-stream locations to allow for individual AIBN pump elements to be fired sequentially. These individual actuators are labeled “Perturb” 1-4. In addition, by applying a no-flow boundary condition to the four perturbations, we will model a standard t-mixer, which may be used to understand the influence of numerical, or artificial, diffusion. Given this problem definition, four variables are chosen for optimization:

1. Pressure amplitude
2. Frequency of perturbation pulse
3. Time delay between opposite actuators (1 & 3, 2 & 4)
4. Time delay between sequential actuators (1 & 2, 3 & 4)

7.4 Boundary conditions and mesh

Well defined boundary conditions are required for accurate modeling and to ensure numerical convergence. For the fluid dynamics simulation, we use the boundary conditions depicted in figure 42:

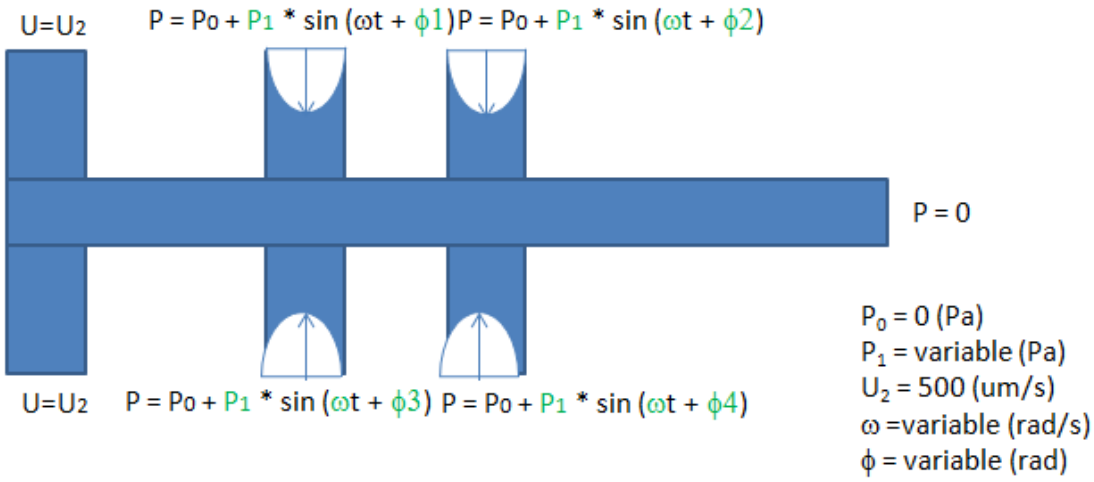

Figure 42: Navier-Stokes boundary conditions

The terms highlighted in green are our optimization variables. For the convection-diffusion equation, the boundary conditions in figure 43 are applied:

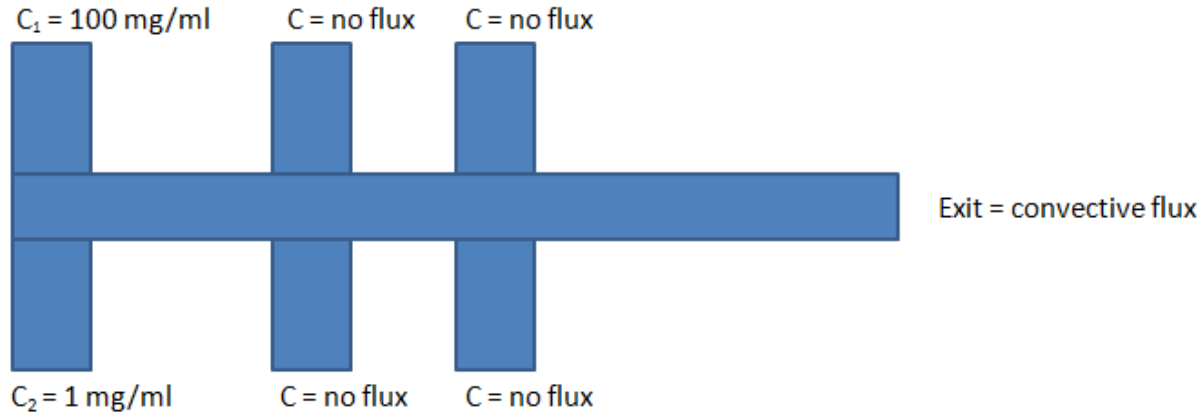

Figure 43: Convection-diffusion boundary conditions

Choosing a proper mesh size is key to both convergence and accuracy of results. Prior researchers have explored the relationship between mesh sizing and accuracy for mixing in the microscale[36, 37]. A consistent theme is the use of artificial diffusion to ensure convergence. Essentially, there may be a tradeoff between simulation convergence and accuracy. We tested a range of mesh sizes to determine computation requirements. All simulations were conducted with the commercial COMSOL multiphysics finite element software. On a HP Elitebook 8470p laptop with an Intel I5-3340M CPU, running at 2.7 GHz with Windows 7 operating system, the following times are required for solution:

Mesh name	Min element length (μm)	Max element length (μm)	Computation time (minutes)
Coarse	2.5	65	52-56
Normal	2	43.5	~210
Fine	1.5	33.5	~1550

These three mesh choices are depicted in Figure 44:

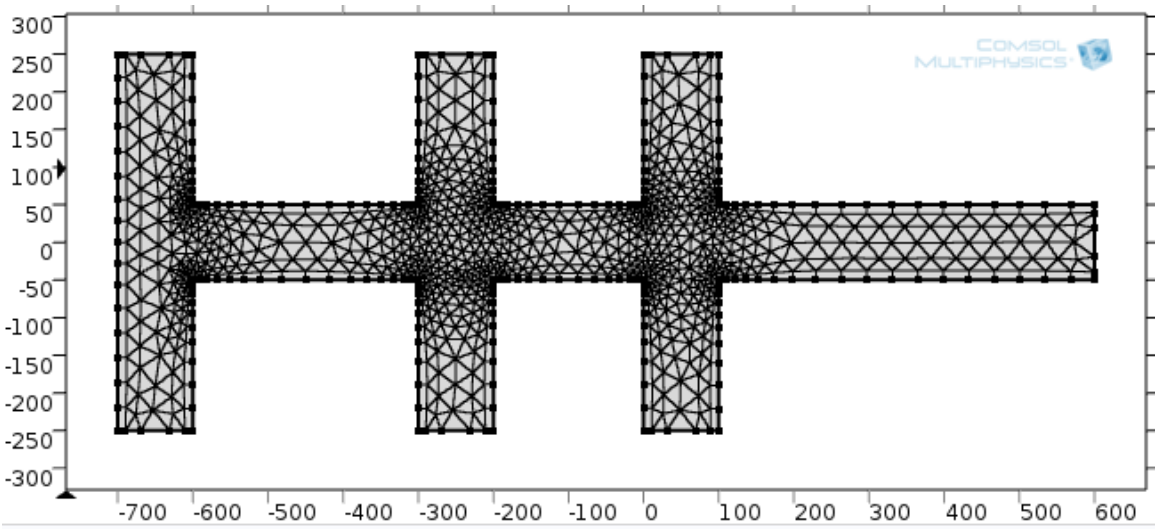

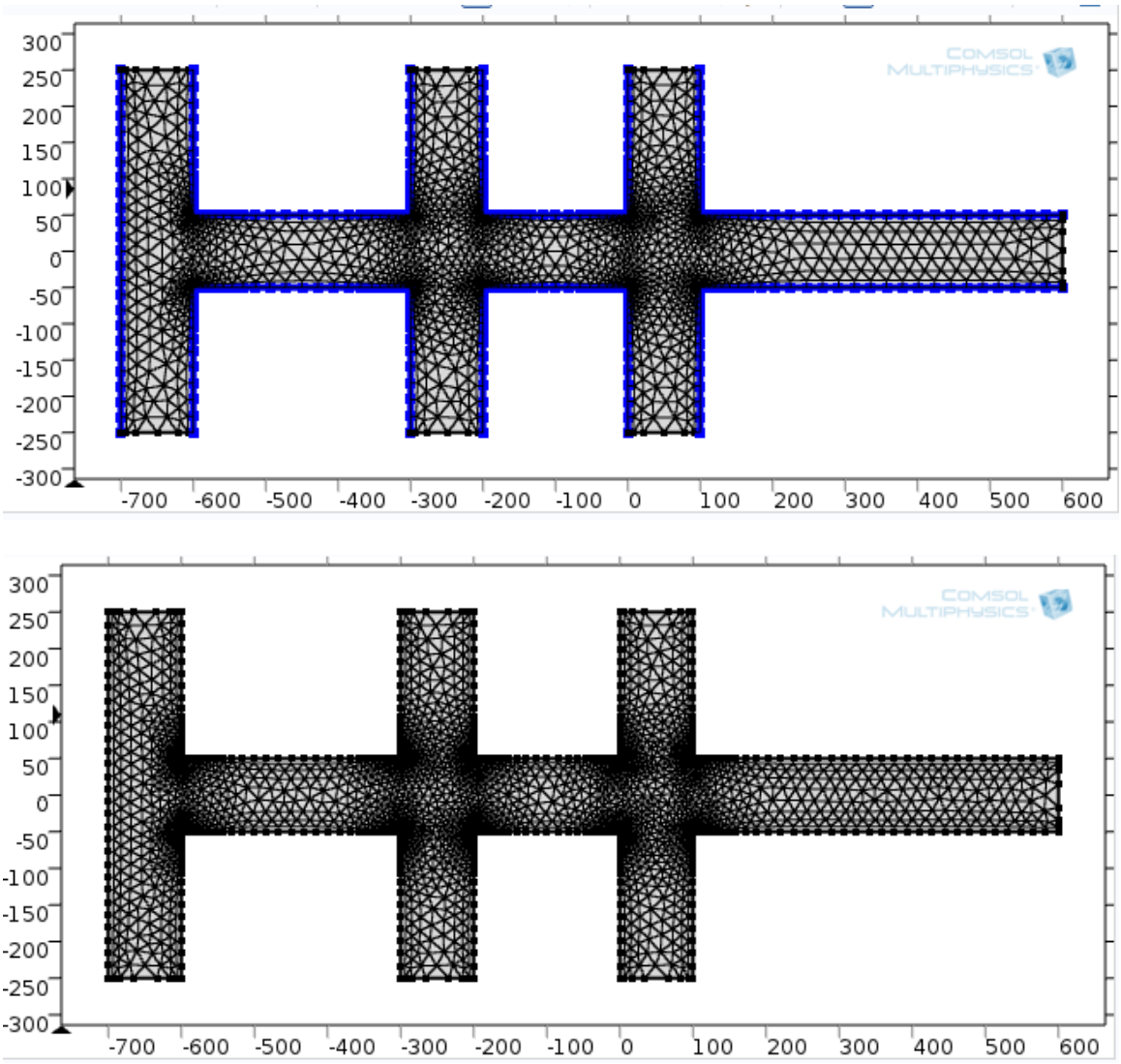

Figure 44: mesh choices for micromixer simulation

Since we are considering four optimization variables, with three levels each to inspect for curvature in the response space, this could require up to 81 runs to fully define the response of the mixing index. Simulations requiring >80 days are not a practical approach to discern the optimal design. Therefore, we will use a combination of Design of Experiment techniques as well as an informed use of meshing to reduce the computation time. To evaluate the effect of

numerical diffusion on the solution, the model was run with no perturbation to simulate a T-mixer for various meshing options, which is shown in Figure 45:

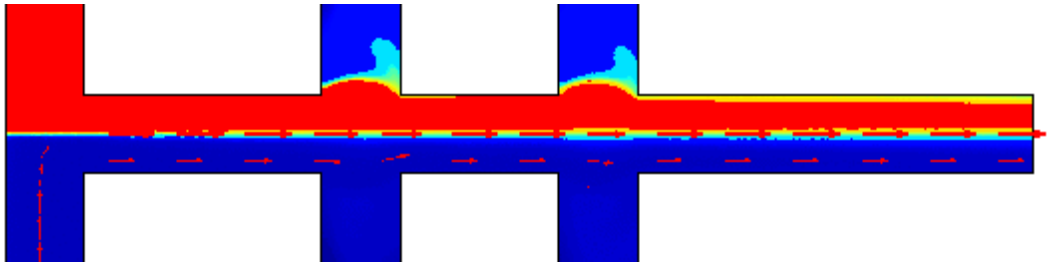

Figure 45: mixer solution at t=20sec for “normal” mesh

The mixing index was calculated for all three mesh choices, and is depicted in Figure 46:

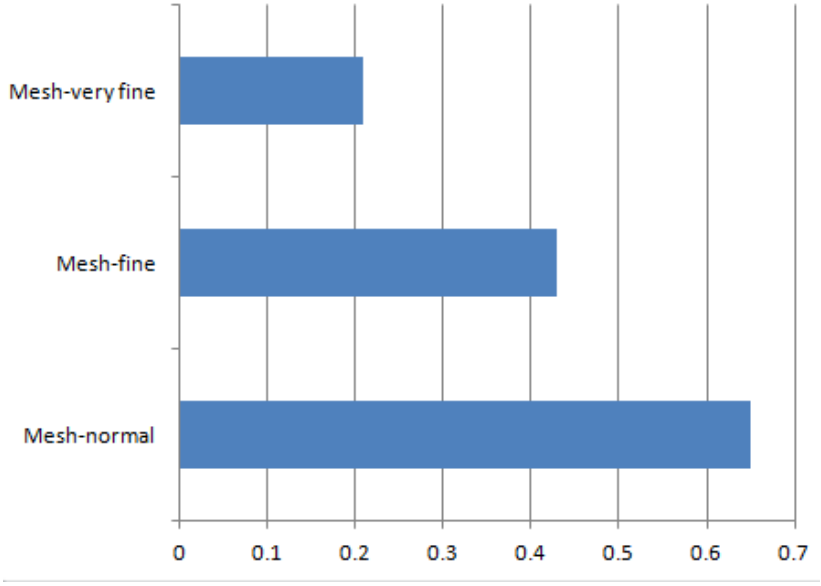

Figure 46 Computed mixing index as a function of mesh size

The experimentally verified for a mixing index at these conditions, as noted in Ref 33, is less than 0.2. Therefore, only a very fine mesh provides sufficient numeric accuracy. We will use a coarse mesh simulation to conduct the Design of Experiments, and then use a refined mesh for the best-case solution, to verify the results and produce more accurate values.

7.5. Taguchi Design of Experiments

Design of Experiments (DOE) is a methodology to correlate one or more independent variables to one or more dependent variables. DOE was first developed to identify potential cures for scurvy. It is now broadly used in engineering practice when a deterministic relationship between the independent variables and dependent variables is not known, or if the relationship is sufficiently complex that an experimental approach will yield insight to system behavior. Our micromixer falls into the second category. After conducting the DOE, the results may be used to minimize variation, or find a local maxima or minima value. Since our system is deterministic, we do not need to repeat runs to look for statistical variation, because there is none.

We have four design variables. Since it is unknown whether the mixing index response to these variables is linear or higher order, we choose to conduct our experiments at three values to assess "curvature" of the mixing index to these variables. If all combinations are tested, 3^4=81 tests are required. Therefore, we seek a more efficient method to identify the optimal micromixer design.

A typical DOE approach is to "confound" different experimental conditions. This means that higher-order interactions, such as between two or more independent variables, are indistinguishable from simpler dependencies. The simpler dependency is assumed to drive behavior. For example, an interaction between three variables may be indistinguishable from a single independent variable, and the single variable is treated as the only dependency.

There are many schemes to design a set of experiments. Typical key elements for a DOE are randomization, replication, orthogonality, and the use of factorial experiments. In our case, randomization and replication are not necessary, since all experiments are not subject to variable

output. Orthogonality ensures that the optimization space is explored with combinations that maximize independence between variables. We seek a highly efficient method to rapidly discern the high-impact variables, to confirm that we have chosen the correct design variables. Two methods, Plankett-Burman and Taguchi, both offer a highly condensed set of runs to quickly assess the influence of the independent variables. We choose to execute a Taguchi DOE, since this methodology is more amendable to future response-surface mapping. Only nine runs are required for our Taguchi. The exact experiments are depicted in appendix C.

7.6 Micromixer Taguchi results

Our design space is depicted in the table below:

Level	Pressure amplitude (Pa)	Frequency (rad/sec)	Phase shift between opposite channels (rad)	Phase shift between adjacent channels (rad)
High	4	2.51	6/5 π	π / 3
Medium	3.5	1.26	π	π / 4
Low	3	0.84	2/3 π	π / 6

The Peclet number for our system is 3226, which indicates advective transport dominates diffusion. As outlined in the initial problem statement, this is by intent. If diffusion is sufficiently high, there is no need for a mixer.

Several simulations were conducted to examine flow behavior. The simulation must be conducted for a sufficient period of time to ensure that the mixer exhibits consistent periodic behavior.

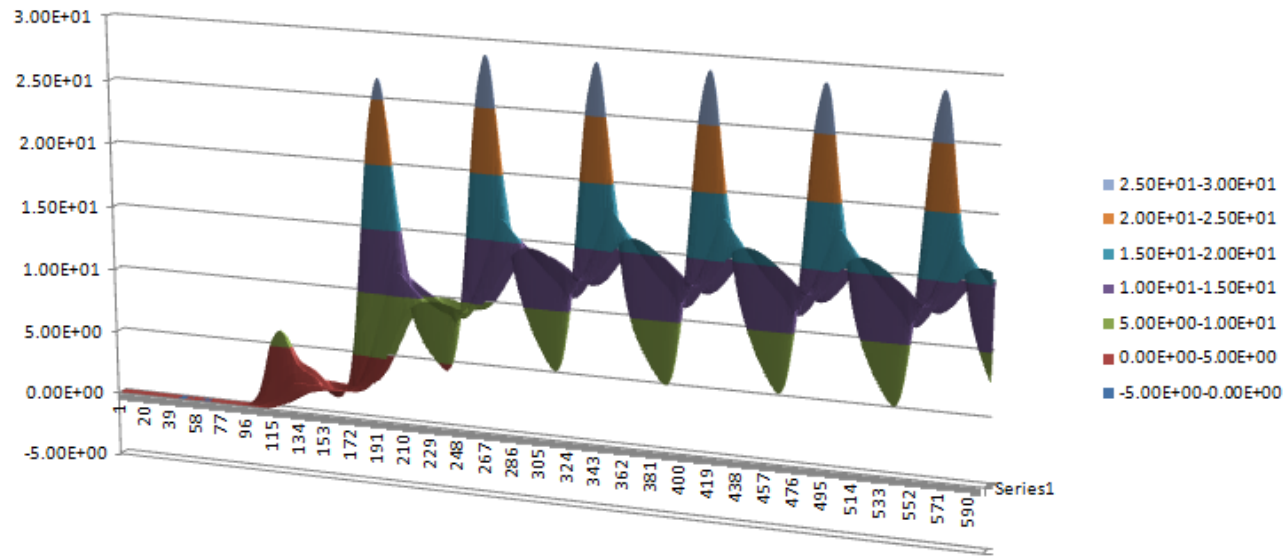

Figure 47: Concentration across exit vs. time. The y-axis is concentration (mol/m^3), the x-axis is time (tenths of a second), and the z-axis is the span of the exit.

Figure 47 depicts the variation of concentration across the exit versus time for Taguchi number 4. The first 10 seconds are required for the perturbed flow to reach the exit. Consistent behavior does not emerge until ~30seconds. Thus, our simulations are conducted for 60 seconds to ensure consistency between runs.

Time resolution was based on the period of the chosen frequencies. Based on multiple simulations, we chose periods of 2.5 to 7.5 seconds to look for inflection in the response surface. To ensure sufficient time resolution, we sample at a rate at least 10x greater than the shortest

period. This time step does not satisfy the Courant-Friedrichs-Lewy (CFL) condition, which may be used as a guide to choosing the time step:

CFL=V* del t / del x <1

However, since COMSOL uses an implicit solver, the CFL criteria may be exceeded. By selecting del t=0.1 seconds, we sample a single period 25 times.

To ensure consistent numerical convergence, we avoid spontaneous discontinuities. In particular, the initial step from a Rhodamine-free flow field resulted in frequent non-convergence. We applied a numerical Heaviside function to ramp the entrance from zero to a non-zero concentration.

The final frame of each of the nine runs is presented with some commentary to inform our understanding of the calculated mixing index averaged across the final period.

Taguchi run #1, was conducted at the low setting for all variables. This results in a strongly differentiated high concentration wave that propagates through the final mixing section. In addition, the concentration is strongly differentiated between Perturb1 and the other 3 actuators.

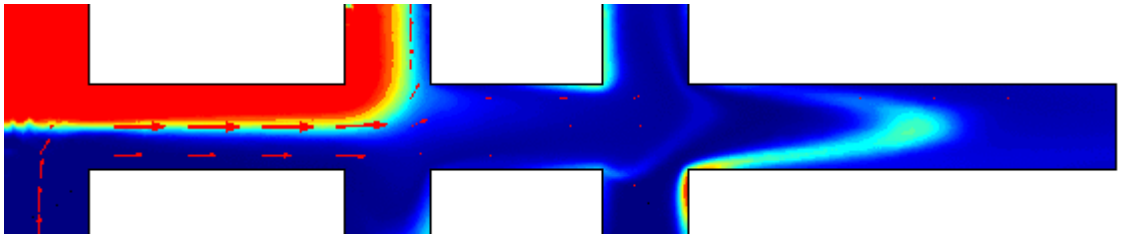

Figure 48: Taguchi 1

Taguchi run #2 retains the low pressure value, but increases the remaining three variables to the midrange value. Note the four actuators are more closely coupled. The high concentration wave still exists, but has been more thoroughly mixed.

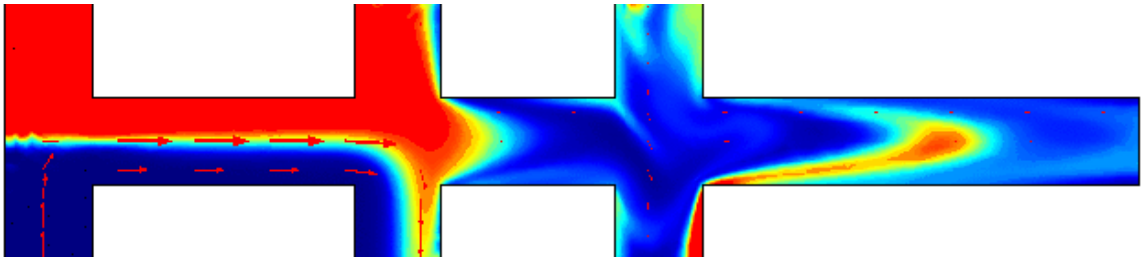

Figure 49: Taguchi 2

Taguchi #3 is run at the low pressure setting, with the remaining three variables at the high setting. Note the rapid folding that occurs between perturb 2 and 4. This results in a well mixed downstream region.

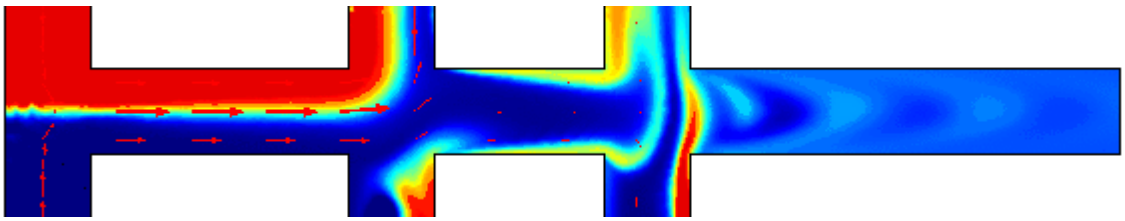

Figure 50: Taguchi 3

Taguchi #4 is run at low firing frequency, and the phase shift between 1/3 and 2/4 results in large regions of unmixed solution.

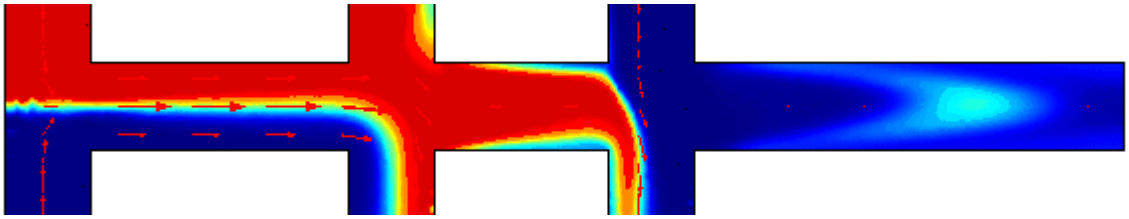

Figure 51: Taguchi 4

Taguchi #5 is an interesting case. Midrange values were used for pressure and firing frequency. High value was used for opposite actuators, but low value was used for adjacent actuators. This results in a clearly defined high concentration wave, but mixing is well established.

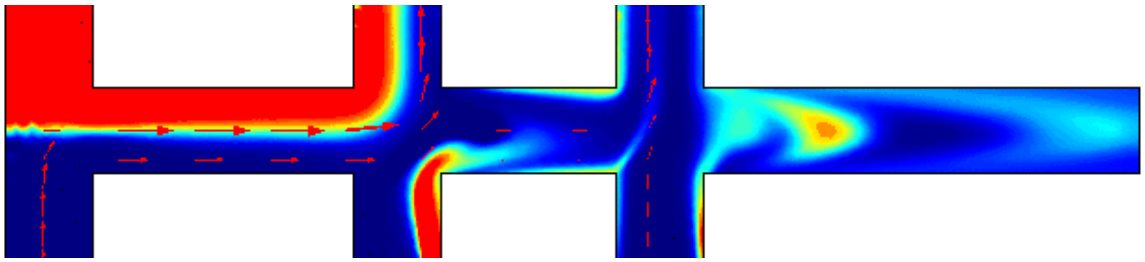

Figure 52: Taguchi 5

Taguchi #6 demonstrates the superior mixing associated with the highest firing frequency. By using the lower values for phase angles, there is less folding than is possible. Overall mixing is high.

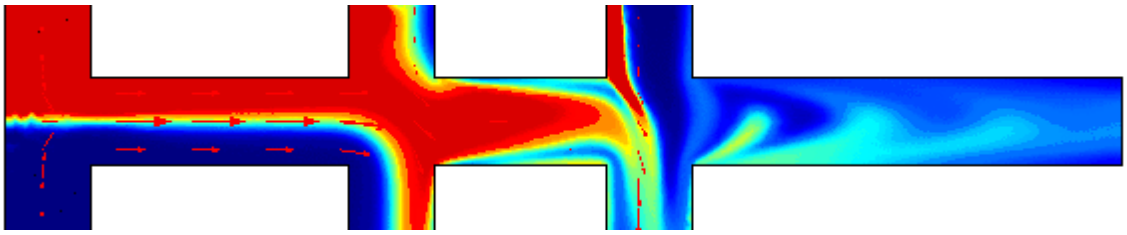

Figure 53: Taguchi 6

Taguchi #7 represents the best potential mixing for the low frequency firing rate. Note the indication of folding in the downstream region.

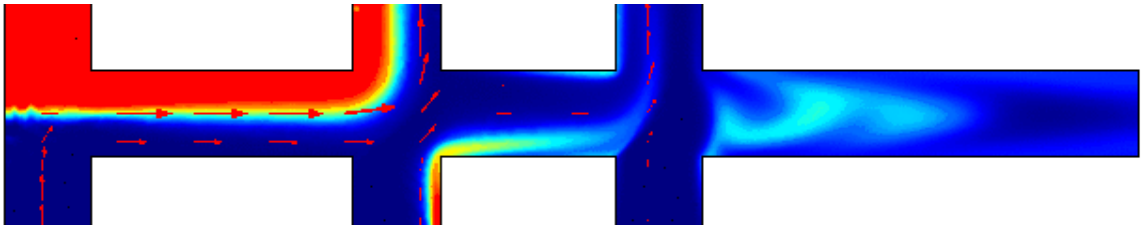

Figure 54: Taguchi 7

Taguchi #8 is conducted at the high pressure setting and the midrange firing frequency. Although there are still clearly distinct high concentration waves, the distance between them is shortened compared to some of the prior runs.

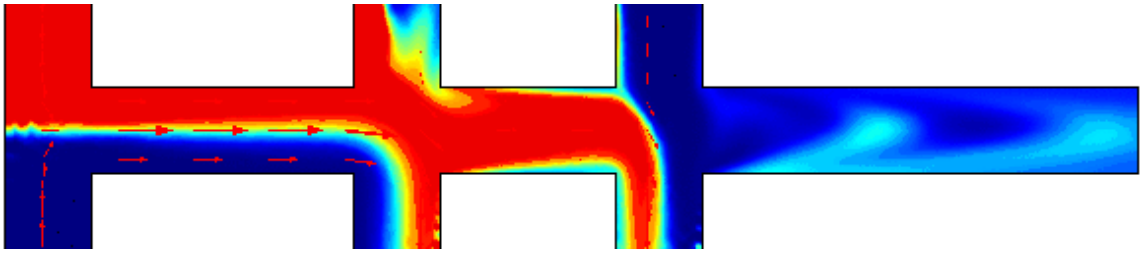

Figure 55: Taguchi 8

Taguchi #9 is run at high frequency and pressure, so we might anticipate that mixing index would be high. Note the downstream section of the mixer. This suggests that the period between high concentration waves is long, and that mixing may not be as high as other runs.

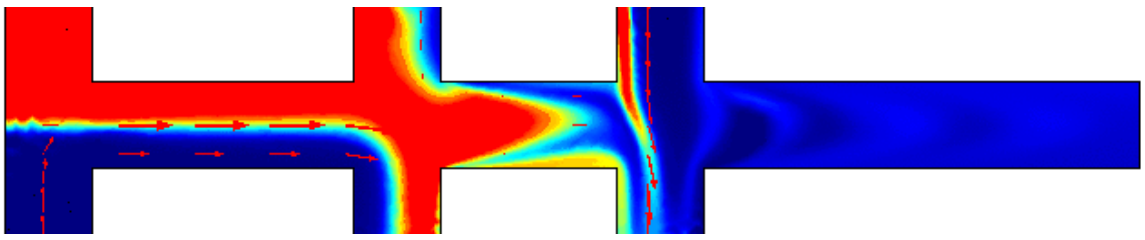

Figure 56: Taguchi 9

After this qualitative review, we conduct a quantitative comparison of the mixing index in the table below:

Taguchi run #	1	2	3	4	5	6	7	8	9
Pressure	3	3	3	3.5	3.5	3.5	4	4	4
Frequency	0.84	1.26	2.51	0.84	1.26	2.51	0.84	1.26	2.51
Strouhal number	0.084	0.126	0.251	0.084	0.126	0.251	0.084	0.126	0.251
Phase shift opposite	2/3 π	π	6/5 π	π	6/5 π	2/3 π	6/5 π	2/3 π	π
Phase shift adjacent	π/6	π/4	π/3	π/3	π/6	π/4	π/4	π/3	π/6
Mixing index	0.72	0.78	0.95	0.65	0.77	0.8	0.75	0.77	0.87

The optimal mixer design, which has the maximum mixing index, is highlighted in green, and the least desirable mixer has the minimum value highlighted in yellow. The Taguchi method allows us to examine the relative influence of each of the independent variables on the mixing index. These are presented in Figure 57:

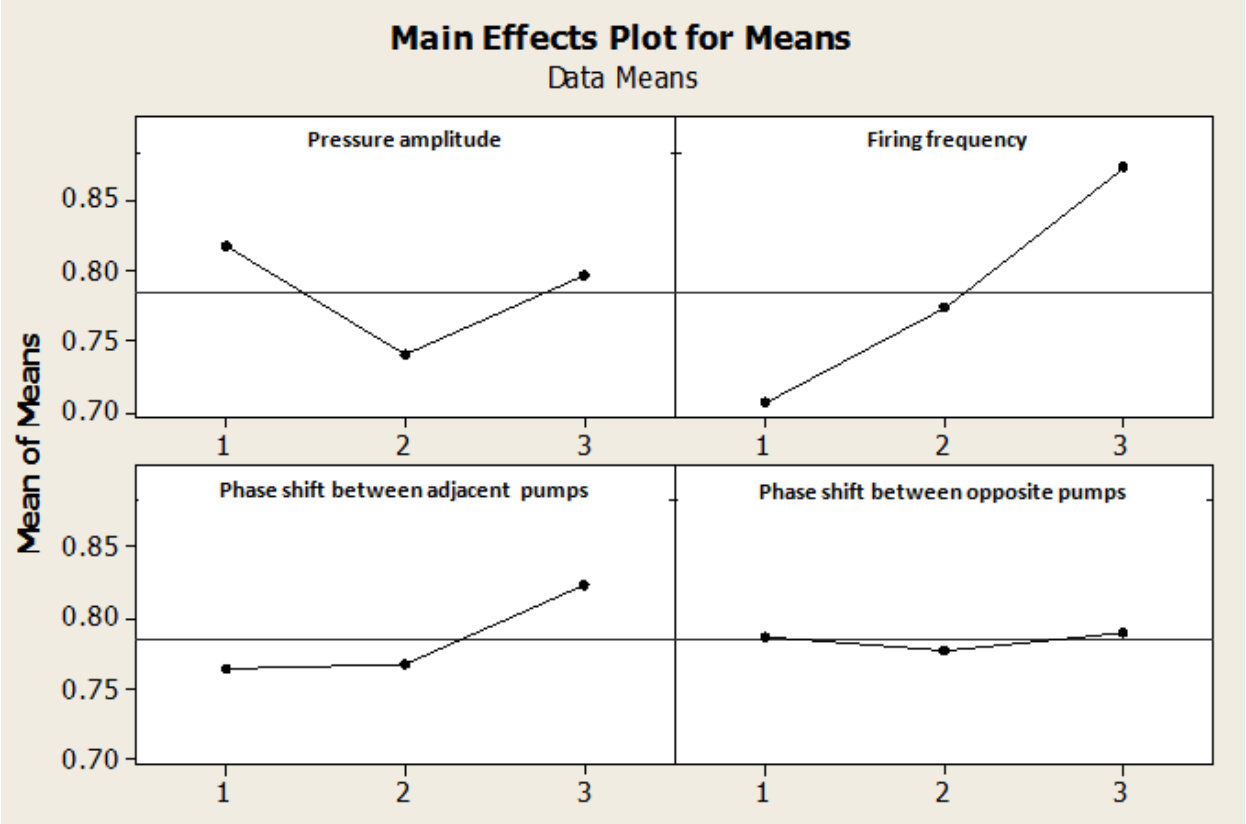

Figure 57: Mixing index dependence on design variables

Several key relationships emerge. The firing frequency has the greatest influence on the mixing index. Increasing the firing frequency strongly increases mixing. Pressure amplitude demonstrates curvature. This validates our choice for three levels for each variable. Interestingly, the mid-range value for pressure amplitude inhibits folding. The two phase shift parameters exhibit some degree of curvature, but are decidedly weaker influences. The phase shift between adjacent actuators shows a stronger dependence than between opposite.

To validate our choice for the optimal micromixer, we require one additional non-dimensional number, the Strouhal number, which is used to describe oscillating flow:

$$\mathrm{St} = \frac{fL}{V}$$

Where f is the frequency of actuator firing, L is the channel width, and V is the inlet velocity. The relationship between mixing index and Strouhal number for pressure-driven flow was experimentally investigated in prior work. The key output from that work is shown in Figure 58:

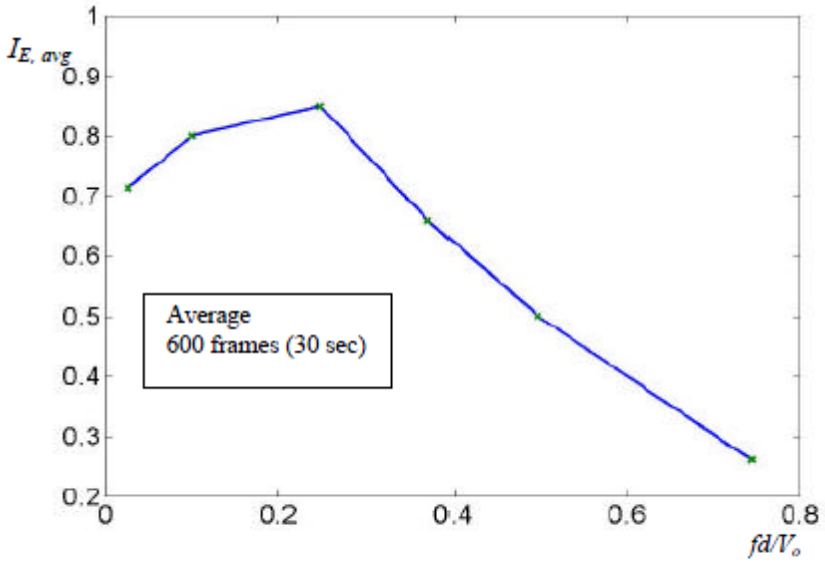

Figure 58: Mixing index vs. Strouhal number, taken from Ref 32

These researchers demonstrated peak mixing at St=0.25, and shows rising values as Strouhal number increases from zero. This agrees with our own numerical results. Taguchi #3, the optimal mixer was re-run at the "fine" mesh condition to achieve more accurate values. Figure 59 illustrates this refined result.

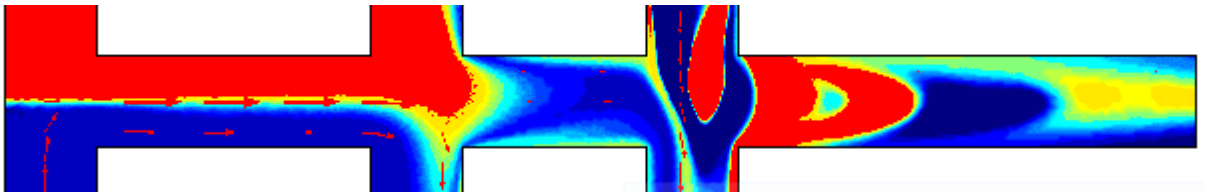

Figure 59: Taguchi #3 with refined mesh

In this case, our mixing index drops to 0.80. We would expect reduced mixing index as our result becomes more accurate. The difference in the absolute value of mixing index between this work and the prior experimental work may be due to driving pressure.

In conclusion, a micromixer has been successfully designed and optimzed via Taguchi Design of Experiments. The key findings of the DOE are supported by prior experimental evidence.

Appendix A: Recrystallization of NIPA

The NIPA monomer is typically shipped with an inhibitor to prevent spontaneous polymerization. This inhibitor must be removed to produce the monomer used in gel experiments.

Measure out 10g of NIPA

Dissolve in 60 mL toluene

Mix until the NIPA completely dissolves

Sit for 10 minutes

Create funnel from #1 Whatmann paper

Pour solution though funnel into new triangular flask

Use ~10 mL toluene to rinse beaker and filter paper

Add 420 mL hexane to filtered product

Sit for 1 hour

Place flask in 4^0 C refrigerator overnight

Retrieve flask, use spatula to break NIPA crystal into manageable chunks

Cut #1 Whatmann down to completely cover the bottom of a Buchner filter

Place Buchner filter at mouth of a vacuum flask

Place NIPA/hexane product into Buchner filter

Use hexane to rinse NIPA on top of the filter, use 2 rinses, wait until no more liquid drains from filter

Put NIPA under vacuum for ~2 hours or until dry

Appendix B: Basic NIPA gel recipes

NIPA gels have been studied by many researchers, and there are a variety of recipes used to fabricate the gel. The relative concentration of NIPA monomer, crosslinker, intiator, and dye will affect the porosity of the gel, strength, and stroke length of the actuator. A basic recipe for gel creation is outlined below. The relative proportions of each are noted by different authors below.

Use 100 mL round bottom flask

Use ice bath to pre-chill flask to prevent premature polymerization

Measure out NIPA and transfer to flask

Measure and add Bis

Measure and add chloropyllin if needed

Use pipette to add TEMED

Measure and add water

Add stir bar to flask, place flak in ice bath, and begin stirring

Use rubber septum to seal flask

Insert N_2 line through septum and into flask

Bubble solution gently with N_2 for 35 minutes

Measure and add ammonium persulphate

Stir 10 more minutes to ensure initiator is dissolved

Gelation will occur-timing depends on temp of bath and concentration of initiator

	Suzuki, ‘90	Li, ‘90	Mitwalli, ‘98
NIPA	7.8 g	7.8 g	0.78 g
Bisacrylamide xlink	670 mg	133 mg	13 mg
Chlorophyllin	0.72 g		
TEMED	240 μL	240 μL	24 μL
Ammonium persulphate	0.2 g	0.004 g	0.0016 g
Water	100 mL	100 mL	100 mL

Appendix C: Taguchi DOE

For a DOE with four independent variables, and three levels, there are 81 potential combinations. These are reduced to 9 runs for a Taguchi DOE. The runs are level combinations are depicted below.

4 factor taguchi, 3 levels

A	B	C	D
1	1	1	1
1	2	2	2
1	3	3	3
2	1	2	3
2	2	3	1
2	3	1	2
3	1	3	2
3	2	1	3
3	3	2	1

References

1. C.-M. Ho, “Fluidics – the link between micro and nano science and technologies”, in Proc. IEEE Micro Electro Mechanical Systems Conf., 2001, pp. 375-384.
2. DA Hoagland, E Arvanitidou, and C Welch, “Capillary electrophoresis measurements of the free solution mobility for several model polyelectrolyte systems”, Macromolecules, vol. 32, pp. 6180-6190, 1999.
3. DE Wroblewski, M Horenstein, N Vandelli, M Velonis, T Bifano. “MEMS micro-valve arrays for fluidic control”. Micro-Electro-Mechanical Systems (MEMS) - 1998. ASME International Mechanical Engineering Congress and Exposition. ASME. 1998, pp.145-51
4. D Beebe, J Moore, J Mauer, Q Yu, R Liu, C Devadoss, and B-H Jo. “Functional hydrogel structures for autonomous flow control inside microfluidic channels”. Nature 404, 588-590 (2000).
5. Q Yu, JM Bauer, JS Moore, DJ Beebe. “Responsive biomimetic hydrogel valve for microfluidics”. Applied Physics Letters, vol.78, no.17, 23 April 2001, pp.2589-91.
6. H Suzuki, T Tokuda, K Kobayashi. “A disposable "intelligent mosquito" with a reversible sampling mechanism using the volume-phase transition of a gel.” Sensors and Actuators B: Chemical, Volume 83, Issues 1-3, 15 March 2002, Pages 53-59
7. TH Wang, PK Wong, and C.-M. Ho, “Electrical molecular focusing for laser induced fluorescence based single DNA detection”, in Proc. IEEE Micro Electro Mechanical Systems Conf., 2002, pp.15-18.

8. T Tanaka, D Fillmore. “Kinetics of swelling of gels”. J. Chem Phys. Vol 70, No. 3. 1214-1218 (1979).
9. EA Vogler, “Structure and reactivity of water at biomaterial surfaces”, Adv Colloid and Interface Sci. 74: 69-117 (1998)
10. J Israelachvilli, H Wennerstrom “Role of hydration and water structure in biological and colloidal interactions” Nature 379: 219-225 (1996)
11. PM Wiggins, RT van Ryn. “Changes in ionic selectivity with changes in density of water in gels and cells” Biophys. J. 58: 585-596 (1990)
12. IL Cameron, KR Cook, D Edwards, GD Fullerton. “A mechanistic view of the non-ideal osmotic and motational behavior of intercellular water” Cell Biol. International 21 (2): 99-113 (1997)
13. W Lee, Polymer Gel Based Actuator: Dynamic Model of Gel for Real Time Control, MIT PhD thesis, 1990
14. A Suzuki, T Tanaka. “Phase transition in polymer gels induced by visible light”. Nature 346, 345-347 (1990).
15. T Ikehara, M Tanakii, S Shimada, H Matsuda. “Optically-driven actuator using photo-induced phase-transition material”. Technical Digest. MEMS 2001. 14th IEEE International Conference on Micro Electro Mechanical Systems, Interlaken, Switzerland, 21-25 Jan. 2001.) Piscataway, NJ, USA: IEEE, 2001. p.256-9
16. S Zhu, AE Hamielec, RH Pelton. 1993. “Modelling of crosslinking and cyclization in free radical copolymerization of vinyl/divinyl monomers” Makromol. Chem. Theory Simul. 2: 587-604

17. Mark, Bikales, Overberger, Menges. “Gels” Second Edition Encyclopedia of Polymer Science and Engineering. Vol. 7, 1985 p. 514-530

18. K Dusek, Responsive Gels Springer-Verlag Berlin Heidelberg 1993.

19. PJ Flory, BD Rehner. 1942. “Statistical mechanics of cross-linked polymer networks” J. Chem. Phys. 11:521-526

20. Y Li, T Tanaka. “Kinetics of swelling and shrinking of gels”. J. Chem. Phys. Vol 92, No. 2. 1365-1371. (1990)

21. E Matsuo, T Tanaka. “Kinetics of discontinuous volume-phase transitions of gels”. J. Chem. Phys. 89 (3) 1695-1703

22. A Mitwalli, Polymer Gel Actuators and Sensors, MIT PhD thesis, 1998

23. A Suzuki, S Yoshikawa, G Bai. **“**Shrinking pattern and phase transition velocity of poly(N-isopropylacrylamide) gel”. Journal of Chemical Physics, vol.111, (no.1), AIP, 1 July 1999. p.360-7. 33 references.

24. D Kuckling, H-Jürgen P. Adler, K-F Arndt , J Hoffmann, M Plötner, T Wolff “Photocrosslinking of thin films of temperature-sensitive polymers” Polymers for Advanced Technologies Volume 10, Issue 6, 1999. 7 Jul 1999

25. G Chen, Y Imanishi, Y Ito. “PH-sensitive thin hydrogel microfabricated by photolithography”. Langmuir 1998, 14, 6610-6612.

26. G Chen, Y Imanishi, Y Ito. “Photolithographic synthesis of hydrogels”. Macromolecules 1998, 31, 4379-4381.

27. L Liang, X Feng, J Liu, P Bieke. "Preparation of Composite crosslinked poly NIPA gel layer and characteristics of reverse hydrophilic/phobic surface". Journal of Applied Polymer Science 1998, 1-11.
28. CC Hong, S Murugesan, S Kim, G Beaucage, JW Choi, CH Ahn. "A functional on-chip pressure generator using solid chemical propellant for disposable lab-ob-a-chip". Lab Chip 2003, 3, 281-286
29. CY Lee, CL Chang, YN Wang, LM Fu. "Microfluidic mixing: a review". International Journal of Molecular Sciences. 2011, 12, 3263-3287.
30. PN Nge, CI Rogers, AT Wooley. "Advances in Microfluidic Functions, Integration, and Applications". Chemical Reviews. 2013, 113, 2550-2583.
31. HM xia, C Shu, SY Wan, YT Chew. "Influence of the Reynolds number on chaotic mixing in a spatially periodic micromixer and its characterization using dynamical system techniques". J. Micromech. Microeng. 16 (2006) 53-61
32. YK Lee, C Shih, P Tabeling, CM Ho. "Experimental study and nonlinear dynamic analysis of time-periodic micro chaotic mixers". J. Fluid Mech. 2007. Vol 575 p 425-448.
33. X Niu, YK Lee. "Efficient spatial-temporal chaotic mixing in microchannels". J. of Micromechanics and Microengineering. 13 (2003) 454-462
34. http://en.wikipedia.org/wiki/Chaotic_Advection
35. JC Sprott. Chaos and time-series analysis p. 115
36. Y Ma, CP Sun, M Fields, Y Li, D Haake, BM Churchill, CM Ho "An unsteady Microfluidic T-form mixer perturbed by hydrodynamic pressure". J. Micromech. Microeng. 18 (2008) 1-14.

37. T Glatzel, C Litterst, C Cupelli, T Lindeman, C Moosman, R niekrawietz, W Strule, R Zengerle, P Koltay. “Computational fluid dynamics software tools for microfluidic applications-a case study” Computers & Fluids 37 (2008) 218-235.